Fluid Phase Equilibria 393 (2015) 7–25

Contents lists available at ScienceDirect

Fluid Phase Equilibria

journal homepage: www.elsevier.com/locate/fluid

General algorithm for multiphase equilibria calculation at given volume, temperature, and moles

Tereza Jindrová, Jiří Mikyška *

Czech Technical University in Prague, Faculty of Nuclear Sciences and Physical Engineering, Department of Mathematics, Trojanova 13, 120 00 Prague 2, Czech Republic

ARTICLE INFO

Article history:
Received 9 June 2014
Received in revised form 6 February 2015
Accepted 9 February 2015
Available online 12 February 2015

Keywords:
Phase equilibrium
Constant-volume flash
Constant-volume stability
Helmholtz energy minimization
Modified Newton method
Modified Cholesky factorization

ABSTRACT

We have developed a fast and robust algorithm for the general Π-phase equilibrium calculation at constant volume, temperature and moles, which is based on the direct minimization of the total Helmholtz energy of the mixture with respect to the mole- and volume-balance constraints. The algorithm uses the Newton–Raphson method with line-search and modified Cholesky decomposition of the Hessian matrix to produce a sequence of states with decreasing values of the total Helmholtz energy. To initialize the algorithm, an initial guess is constructed using the results of constant-volume stability testing. As the number of phases is not known a priori, the proposed strategy is based on repeated constant-volume stability testing and constant-volume phase-split calculation until a stable Π-phase state is found. The performance of the algorithm is shown on several examples of two-, three- and even four-phase equilibrium calculations of multicomponent mixtures under various conditions.

1. Introduction

Studying multiphase equilibrium of multicomponent mixtures and development of robust and efficient algorithms for its computation play important roles in large-scale compositional hydrocarbon reservoir simulations. While there was a main focus on two-phase compositional modelling in the past, nowadays, there is an increasing interest in three and generally multi-phase compositional models which is motivated by CO_2 sequestration [12], processes related to CO_2 or steam enhanced oil recovery [1] or asphaltene precipitation from bitumens [14,15].

Injecting a pure component (e.g. CO_2) into a reservoir, it may dissolve in the reservoir fluid or it can mix and the mixture can split into two or more phases. Let us consider a closed system of total volume V containing a multicomponent mixture with mole numbers $N_1, \ldots, N_n$ at temperature T. To find out whether the system is under given conditions in single-phase or splits into two phases, the single-phase stability at constant volume, temperature, and moles (the so-called *VT*-stability) is solved. In case of phase-splitting, the two-phase split calculation at constant volume, temperature, and moles (the so-called *VT*-flash) is performed to establish amounts and compositions of both phases, and consequently the equilibrium pressure of the system is calculated from the equation of state. In our previous work [22,23,9], these problems were formulated for two-phase systems and the algorithms were proposed and tested on a number of examples. In [10], the results were partially extended to three phases for CO_2–H_2O system and the performance of the algorithm was shown on several examples of two- and three-phase equilibrium calculations of CO_2–H_2O mixtures under geologic carbon storage conditions. In this work, we extend the method and propose a general strategy for Π-phase equilibrium computation at constant volume, temperature, and moles, where $\Pi \in N$ is the number of phases.

We use the formulations of phase stability and phase equilibrium computation which are based on *VT* variables (constant volume, temperature, and moles). This approach is alternative to the traditional formulation based on *PT* variables (constant pressure, temperature and chemical composition), which has been widely used in many applications including compositional reservoir simulation. Both the stability testing and the phase-split computation can be formulated either as local or global minimization problems, or as problems of direct solution of a nonlinear system of algebraic equations. Depending on the problem formulation and used variables, various methods have been developed to find the local minima and the global minimum of the tangent-plane-distant function in the stability testing [17,19,6], and the global minimum of either the Gibbs energy [18,6,16], or the Helmholtz energy [22,9] in computation of phase-equilibria. The reader is referred to [32] for a recent review of various global optimization methods for phase equilibrium calculations.

* Corresponding author. Tel.: +420 224358553.
E-mail address: jiri.mikyska@fjfi.cvut.cz (J. Mikyška).

http://dx.doi.org/10.1016/j.fluid.2015.02.013
0378-3812/

Besides the *PT*-formulations, formulations involving other independent variables appear in the literature. The formulations in which temperature and concentrations are the independent variables were used by Nagarajan et al. in [26] for the investigation of phase stability and flash equilibrium calculation, and in [27] for the critical point calculation. Using volume as an independent variable in the *PT*-flash has also been shown advantageous by Pereira et al. in [29]. Although in these works the independent variables are temperature and concentrations or temperature, volume, and moles, respectively, the problem specification variables are still pressure, temperature, and composition. No matter how wide-spread the use of the *PT*-specification variables is, this approach has limitations which have already been noticed in the previous work. In the *PT*-variables specification, pressure is specified and volume is computed by inverting of the equation of state. In case of cubic equations of state (e.g. the Peng–Robinson EOS), the problem of multiple roots of the equation occurs; there may exist up to three different roots from which one is selected, usually the one with the lowest value of the Gibbs energy. In contrast, in the *VT*-approach volume of the cell is given and pressure can be directly computed from the equation of state without the need for inversion of the equation of state. In the *VT*-formulation, the problem of root selection is completely avoided. This is even more important when using non-cubic equation of state (e.g. the Cubic-Plus-Association EOS) for which the number of roots is not known a priori.

To illustrate another shortcoming of *PT* variables, let us consider pure CO_2 at temperature $T = 280$ K and saturation pressure $P_{sat}(T)$ corresponding to the temperature $T = 280$ K. Using the *PT* variables, one cannot decide whether the system occurs in vapor or liquid state, or as a mixture of both, because all two-phase states and both saturated gas and saturated liquid occur at the same pressure $P_{sat}(T)$, temperature, and moles. Therefore, *PT*-stability and *PT*-flash cannot distinguish between these states, but *VT*-stability and *VT*-flash can, because these states have different volumes. This example shows that the *PT*-stability and *PT*-flash problems are not well posed since the volume of the system is not uniquely determined by specifying the pressure, temperature, and moles. On the other hand, if volume, temperature, and moles are specified, the equilibrium pressure is given uniquely by the equation of state. The ambiguity of volume is not limited to pure component. In [10] and in this work, we present non-trivial examples of multicomponent mixtures which exhibit in three- or even four-phase the same behaviour as the pure substances at saturation pressure.

The phase stability testing and phase equilibrium calculation are the integral part of the reservoir simulation. In compositional models the stability and flash formulations are based virtually exclusively on the *PT*-variables specification [4,8,21,24,25]. To the best of our knowledge, the only use of the *VT*-flash in compositional simulation has been reported in [30]. In [30] there is an example which the codes based on the *PT*-variables specification generally fail to compute because of the ambiguity in volume for given pressure, temperature, and overall composition. In the *VT*-flash formulation, the problem does not appear at all. This motivates our interest in the phase equilibrium calculation using the *VT*-variables specification that does not suffer from these issues.

To solve phase equilibria in other variables specifications (like *VT* in our case), Michelsen [20] proposed an approach based on nested iterations; the *PT*-flash algorithm is used in the inner loop while pressure is iterated in the outer loop until the correct pressure value is found for which the respective volume constraint is satisfied. This approach was used in [5] to find the conditions of thermodynamic equilibrium in systems subject to gravitational fields and in [3] to study segregation in centrifugal fields. This approach allows to reuse existing implementations of the *PT*-flash but is not computationally efficient since for a single computation of the *VT*-flash many computations of the *PT*-flash have to be performed before the correct value of pressure is found. In [22] it has been shown that when the *VT*-flash problem is formulated directly using the minimization of the Helmholtz energy, the computational efficiency of the successive iteration method is about the same as for its *PT*-based counterpart. Moreover, as the nested loop approach uses the *PT*-flash in the inner loop, the method may not provide the correct phase volumes when the volume is ambiguous.

In [9] we have proposed a numerical algorithm for constant-volume two-phase split calculation which is based on the constrained minimization of the total Helmholtz energy of the mixture. The algorithm uses the Newton–Raphson method with line-search and the modified Cholesky decomposition of the Hessian matrix to produce a sequence of states with decreasing values of the total Helmholtz energy. Fast convergence towards the exact solution is ensured due to the Newton–Raphson method. Furthermore, as the method guarantees decrease of the total Helmholtz energy of the system in every iteration, it always converges to a state corresponding to at least a local minimum of the energy. To initialize the algorithm, the results of the constant-volume stability algorithm, which has been developed in [23], are used. In this work, we extend the method and propose a general strategy for Π-phase equilibrium computation at constant volume, temperature, and moles, where $\Pi \in N$ is the number of phases. As the number of phases is not necessarily known a priori, the proposed strategy is based on the repeated constant-volume stability testing and the constant-volume phase-split calculation until a stable Π-phase state is found. The performance of the algorithm is shown on several examples of two-, three- and even four-phase equilibrium calculations of multicomponent mixtures under various conditions. The basic approach adopted here is close to that of Cabral et al. [2] where the direct minimization of the Helmholtz energy is used to solve thermodynamic equilibrium in a system with various bulk and adsorbed phases. However, in [2] the authors claim that because pressure can be negative during the course of the iterations, their algorithm requires that a part of the computation be performed in the complex arithmetics. On the other hand, our algorithm uses formulation that can be performed in the real arithmetic. The use of complex numbers is thus avoided.

The paper is structured in the following way. In Section 2, we derive the equilibrium conditions in a multiphase system which is described using the Helmholtz energy. In Section 3, the constant-volume stability testing is applied on a multicomponent mixture in a Π-phase state and a method of introducing a new phase is described in the case that the Π-phase state is unstable and splits into $\Pi + 1$ phases. Finally, we propose a fast and robust numerical algorithm for the multiphase split calculation based on the direct minimization of the total Helmholtz energy of the Π-phase system. At the end of the section, we summarize essential steps of the algorithm and propose the general strategy for constant-volume phase-equilibria computation based on repeated stability testing and phase-split calculations. In Section 4, we present several numerical examples showing the performace, robustness and efficiency of the proposed strategy for multiphase equilibrium computation at constant volume, temperature, and moles. In Section 5, we discuss the results and draw some conclusions. In Appendix A, we provide details of the Peng–Robinson and Cubic-Plus-Association equations of state [28,13] that were used in this work. In Appendix B, we provide the details of the modified Cholesky factorization that is used in our method.

2. Multiphase equilibrium conditions for multicomponent system

Consider a closed system containing a mixture of n components with mole numbers $N_1, \ldots, N_n$ occupying total volume V at temperature T. The system is described using the Helmholtz energy

$A = A(V, T, N_1, \ldots, N_n)$. Let us assume that the mixture occurs in a Π-phase state, where $\Pi \in N$, and denote the volumes of each phase V_α and the mole numbers of each component in each phase $N_{\alpha,i}$, where $\alpha = 1, \ldots, \Pi$ and $i = 1, \ldots, n$. The point is to derive conditions of Π-phase equilibrium in the mixture.

Let us denote by $\mathbf{x}_0$ and $\mathbf{x}_\alpha$ vectors with components $N_1, \ldots, N_n$, V and $N_{\alpha,1}, \ldots, N_{\alpha,n}, V_\alpha$, where $\alpha = 1, \ldots, \Pi$, respectively. Then, for a single-phase system, the Helmholtz energy is given by

$$A^{\mathrm{I}} = A(\mathbf{x}_0, T) = -PV + \sum_{i=1}^{n} N_i \mu_i, \tag{1}$$

where $P = P(\mathbf{x}_0, T)$ is the pressure given by a pressure-explicit equation of state, and $\mu_i = \mu_i(\mathbf{x}_0, T)$ is the chemical potential of the i-th component in the mixture. For the Π-phase system, the total Helmholtz energy reads as

$$A^{\Pi} = \sum_{\alpha=1}^{\Pi} A(\mathbf{x}_\alpha, T). \tag{2}$$

The equilibrium state of the Π-phase system is the state for which the increase in the total Helmholtz energy with respect to an energy reference state given by

$$\Delta A = \sum_{\alpha=1}^{\Pi} A(\mathbf{x}_\alpha, T) - A^{ref}, \tag{3}$$

where the energy reference state A^{ref} can be chosen for example as a single-phase state or a $(\Pi - 1)$-phase equilibrium state, is minimal among all states satisfying the following constraints expressing the volume balance and mole balance

$$\sum_{\alpha=1}^{\Pi} V_\alpha = V, \tag{4}$$

$$\sum_{\alpha=1}^{\Pi} N_{\alpha,i} = N_i, \quad i = 1, \ldots, n. \tag{5}$$

Using the Lagrange multiplier method, the system of $(n+1)$ necessary conditions of Π-phase equilibrium is derived

$$P(\mathbf{x}_1, T) = \cdots = P(\mathbf{x}_\Pi, T), \tag{6}$$

$$\mu_i(\mathbf{x}_1, T) = \cdots = \mu_i(\mathbf{x}_\Pi, T), \quad i = 1, \ldots, n. \tag{7}$$

3. Numerical algorithm for computation of multiphase equilibrium for multicomponent system

In the previous work [22,23,9], we dealt with the single-phase stability analysis and the two-phase split calculation, both at constant volume, temperature, and moles. Now, we extend these results and present a general strategy for Π-phase equilibrium computation at constant volume, temperature, and moles in a multicomponent mixture, where $\Pi \in N$ is the number of phases which is now not known a priori. The proposed strategy is based on repeated constant-volume stability testing and constant-volume phase-split calculation until the stability analysis decides about a stable Π-phase state.

Suppose we have a Π-phase equilibrium state of a multicomponent mixture which is in a closed cell of given volume at a specified temperature. We are interested to find out whether the Π-phase state is stable or unstable splitting into $\Pi + 1$ phases. This is the problem of Π-phase stability investigation at constant volume, temperature, and moles. In the case of phase-splitting we want to establish equilibrium properties of each of the $\Pi + 1$ phases, i.e. chemical composition, mass densities and amounts (volumes) of each phase, and consequently the equilibrium pressure from the equation of state. This is the problem of general multiphase split calculation at constant volume, temperature, and moles.

3.1. Multiphase stability testing

Multiphase stability testing is needed to examine whether the mixture is stable in a given Π-phase state. It can be proven that testing the stability of an Π-phase equilibrium state is thermodynamically equivalent to the single-phase stability testing of any of the Π equilibrium phases [11,6].

The constant-volume single-phase stability test from [23] decides whether the single phase is stable or not at given volume, temperature, and moles. The stability investigation is based on testing trial phases of different compositions in order to find out if there is a composition for which transfer of a small amount of the trial phase from the initial phase causes a decrease in the Helmholtz energy. The criterion of stability at constant volume, temperature, and moles is formulated using the so-called tangent plane distance D function (see [23] for details). The single phase is stable if

$$D(T, c'_1, \ldots, c'_n) = \lim_{V' \to 0+} \frac{\Delta A}{V'} = \sum_{i=1}^{n} \left[\mu_i(c'_1, \ldots, c'_n, 1, T) - \mu_i(c_1, \ldots, c_n, 1, T)\right] c'_i - \left[P(c'_1, \ldots, c'_n, 1, T) - P(c_1, \ldots, c_n, 1, T)\right] \geq 0 \tag{8}$$

for all admissible states $(T, c'_1, \ldots, c'_n)$. If this condition is satisfied, the system is in single-phase and the VT-flash calculation is avoided. If a trial phase composition is found such that the D function is negative, the mixture is unstable and splits into two phases. In the two-phase case, concentrations of the trial phase, for which the value of D is negative, can be found using the algorithm from [23] and used in the construction of an initial guess for the phase-split calculation.

3.2. Introduction of a new phase

If a multicomponent mixture of n components occurs in an unstable Π-phase state and splits into $\Pi + 1$ phases, an initial $(\Pi + 1)$-phase split is needed to initialize the phase-equilibrium computation. Using the stability algorithm from [23], a trial phase with molar concentrations c'_i for which the D function is negative is found such that, if taken in a small amount from the initial Π phases, the $(\Pi + 1)$-phase split composed of the trial phase and the other Π phases will have lower total Helmholtz energy than the initial Π-phase system. We are interested in finding the initial phase-split and establish its phase properties.

Assume that the initial unstable Π-phase state is described by the volumes of each phase V_α and the mole numbers of each component in each phase $N_{\alpha,i}$, where $\alpha = 1, \ldots, \Pi$ and $i = 1, \ldots, n$, and the $(\Pi + 1)$-phase split is described by the volumes V', V^*_α and the mole numbers $N'_i, N^*_{\alpha,i}$, where the prime variables represent the trial phase and *-variables represent the other Π phases, respectively. Let us introduce for the initial Π-phase system the molar concentrations of each component $c_{\alpha,i} = N_{\alpha,i}/V_\alpha$ and the volume fractions $S_\alpha = V_\alpha/V$ satisfying the volume- and mole-balance constraints in the following form

$$\sum_{\alpha=1}^{\Pi} S_\alpha = 1 \quad \text{and} \quad \sum_{\alpha=1}^{\Pi} S_\alpha c_{\alpha,i} = c_i, \quad i = 1, \ldots, n. \tag{9}$$

Further, let us denote the molar concentrations of each component in the trial phase and in each of the other Π phases, forming together the $(\Pi + 1)$-phase split, by $c'_i = N'_i/V'$ and $c^*_{\alpha,i} = N^*_{\alpha,i}/V^*_\alpha$, respectively, and the volume fractions of the trial phase and each

of the other Π phases by $S' = V'/V$ and $S^*_\alpha = V^*_\alpha/V$, respectively. Suppose we transfer the same amounts of each component from each of the Π equilibrium phases to form the new trial phase, then the constraints (9) can be rewritten as

$$\sum_{\alpha=1}^{\Pi} \underbrace{(S_\alpha - \frac{1}{\Pi}S')}_{S^*_\alpha} + S' = 1 \qquad \text{and} \qquad \sum_{\alpha=1}^{\Pi} \underbrace{(S_\alpha c_{\alpha,i} - \frac{1}{\Pi}S'c'_i)}_{S^*_\alpha c^*_{\alpha,i}} + S'c'_i = c_i,$$

$i = 1, \ldots, n.$

From the last equation, the molar concentrations of each component $c^*_{\alpha,i}$ and the volume fractions S^*_α in each phase of the $(\Pi+1)$-phase split except the trial phase read as

$$S^*_\alpha = S_\alpha - \frac{1}{\Pi}S' \qquad \text{and} \qquad c^*_{\alpha,i} = \frac{S_\alpha c_{\alpha,i} - \frac{1}{\Pi}S'c'_i}{S_\alpha - \frac{1}{\Pi}S'},$$

$$\alpha = 1, \ldots, \Pi, i = 1, \ldots, n \tag{10}$$

satisfying the following constraints

1. $S^*_\alpha \in (0; 1)$,
2. $c^*_{\alpha,i} > 0$,
3. $\sum_{i=1}^{n} c^*_{\alpha,i} b_i < 1$,

where b_i is the parameter from the Peng–Robinson equation of state. Substituting (10) to the constraints, we obtain the following restrictions on the volume fraction of the trial phase S'

$$S' > 0, \quad S' < \Pi \frac{S_\alpha c_{\alpha,i}}{c'_i}, \alpha = 1, \ldots, \Pi, i = 1, \ldots, n \tag{11}$$

$$S' < \Pi S_\alpha, \quad S' < \Pi S_\alpha \frac{1 - \sum_{i=1}^{n} c_{\alpha,i} b_i}{1 - \sum_{i=1}^{n} c'_i b_i}, \alpha = 1, \ldots, \Pi. \tag{12}$$

As the volume fraction of the trial phase is found to satisfy the restrictions (11) and (12), the volume V' is given by $V' = S'V$ and the bisection method can be used to reduce $V'>0$ such that $\Delta A = A^{\Pi+1} - A^{\Pi} < 0$ for a $(\Pi+1)$-phase state in which one phase is the trial phase with volume V' and mole numbers $N'_i = c'_i V'$ and the other Π phases with volumes $V^*_\alpha = S^*_\alpha V$ and mole numbers $N^*_{\alpha,i} = c^*_{\alpha,i} V_\alpha$ are computed such that (4) and (5) hold. This way we have constructed a $(\Pi+1)$-phase state with lower total Helmholtz energy than the initial Π-phase state.

3.3. Numerical algorithm for multiphase equilibrium computation

Assume that a mixture of n components which occurs in an unstable $(\Pi-1)$-phase state at given conditions splits into Π phases. We are interested in establishing equilibrium phase properties, i.e. volumes of each phase V^*_α and mole numbers of each component in each phase $N^*_{\alpha,i}$, where $\alpha = 1, \ldots, \Pi$ and $i = 1, \ldots, n$. Finally, the equilibrium pressure of the system is calculated from the equation of state.

As an initial Π-phase split can be constructed as described above, now we derive a numerical algorithm for calculation of the Π-phase equilibrium at constant volume, temperature, and moles based on the direct minimization of the Helmholtz energy increase with respect to an initial Π-phase split satisfying the volume- and mole-balance constraints (4) and (5). In the following, we denote by $\mathbf{x}_\alpha$ a vector with components $N_{\alpha,1}, \ldots, N_{\alpha,n}, V_\alpha$ and by $\mathbf{x}^*_\alpha$ a vector with components $N^*_{\alpha,1}, \ldots, N^*_{\alpha,n}, V^*_\alpha$, where $\alpha = 1, \ldots, \Pi$. Similarly to the algorithm presented in [9], the numerical procedure is based on transferring an n-dimensional problem of minimization of a twice-continuously differentiable objective function subject to a set of t linear equality constraints into an unconstrained minimization problem with the same objective function, but a lower dimension $n - t$. The constraint equations (4) and (5) can be written in the matrix form as $\mathbb{A}\mathbf{x} = \mathbf{b}$, or

$$\underbrace{\begin{pmatrix} \mathbb{I}_{n+1} & \cdots & \mathbb{I}_{n+1} \end{pmatrix}}_{\mathbb{A}} \underbrace{\begin{pmatrix} \mathbf{x}_1 \\ \vdots \\ \mathbf{x}_\Pi \end{pmatrix}}_{\mathbf{x}} = \underbrace{\begin{pmatrix} N_1 \\ N_2 \\ \vdots \\ N_n \\ V \end{pmatrix}}_{\mathbf{b}}, \tag{13}$$

where $\mathbb{A} \in \mathbf{R}^{(n+1)\times\Pi(n+1)}$ is the matrix formed by Π blocks of the identity matrix in $\mathbf{R}^{n+1}$ which is denoted by $\mathbb{I}_{n+1}$, $\mathbf{x} \in \mathbf{R}^{\Pi(n+1)}$ is the vector of unknowns, which is given as

$$\mathbf{x} = \left(N_{1,1}, \ldots, N_{1,n}, V_1, \ldots, N_{\Pi,1}, \ldots, N_{\Pi,n}, V_\Pi\right)^T$$

and $\mathbf{b} \in \mathbf{R}^{n+1}$ is the vector of right hand side. As the matrix $\mathbb{A}$ has the full rank, the optimization problem with $\Pi(n+1)$ unknowns and $n+1$ linearly independent linear constraints can be transformed into an unconstrained problem with $\Pi(n+1) - (n+1) = (\Pi-1)(n+1)$ variables. The reduction in dimensionality can be described in terms of two subspaces $\mathcal{Y}$ and $\mathcal{Z}$, where $\mathcal{Y}$ is the $(n+1)$-dimensional subspace of $\mathbf{R}^{\Pi(n+1)}$ spanned by the rows of matrix $\mathbb{A}$ and $\mathcal{Z}$ is $(\Pi-1)(n+1)$-dimensional subspace of $\mathbf{R}^{\Pi(n+1)}$ of vectors orthogonal to the rows of matrix $\mathbb{A}$. The representation of $\mathcal{Y}$ is not unique and it can be chosen for example as $Y = \mathbb{A}^T$. As $\mathcal{Y}$ and $\mathcal{Z}$ define complementary subspaces

$$\mathbf{R}^{\Pi(n+1)} = \mathcal{Y} \oplus \mathcal{Z}, \tag{14}$$

every $\Pi(n+1)$-dimensional vector $\mathbf{x}$ can be uniquely written as a combination of vectors from $\mathcal{Y}$ and $\mathcal{Z}$ as

$$\mathbf{x} = \mathbb{Y}\mathbf{x}_\mathcal{Y} + \mathbb{Z}\mathbf{x}_\mathcal{Z}, \tag{15}$$

where $\mathbb{Y}$ and $\mathbb{Z}$ denote matrices from $\mathbf{R}^{\Pi(n+1)\times(n+1)}$ and $\mathbf{R}^{\Pi(n+1)\times(\Pi-1)(n+1)}$, respectively, whose columns represent bases of subspaces $\mathcal{Y}$ and $\mathcal{Z}$, respectively, and the $(n+1)$-dimensional vector $\mathbf{x}_\mathcal{Y}$ is called the range-space part of $\mathbf{x}$, and the $(\Pi-1)(n+1)$-dimensional vector $\mathbf{x}_\mathcal{Z}$ is called the null-space part of $\mathbf{x}$.

The solution $\mathbf{x}^*$ of the constrained optimization problem, given by

$$\mathbf{x}^* = \mathbb{Y}\mathbf{x}^*_\mathcal{Y} + \mathbb{Z}\mathbf{x}^*_\mathcal{Z},$$

is feasible, whence

$$\mathbb{A}\mathbf{x}^* = \mathbb{A}(\mathbb{Y}\mathbf{x}^*_\mathcal{Y} + \mathbb{Z}\mathbf{x}^*_\mathcal{Z}) = \mathbf{b}.$$

From the definition of the subspace $\mathcal{Z}$ it follows that $\mathbb{A}\mathbb{Z} = 0$, therefore

$$\mathbb{A}\mathbb{Y}\mathbf{x}^*_\mathcal{Y} = \mathbf{b}.$$

From the definition of subspace $\mathcal{Y}$, the matrix $\mathbb{AY}$ is non-singular, and thus from the previous equation the vector $\mathbf{x}^*_{\mathcal{Y}}$ is uniquely determined. Similarly, any feasible vector $\mathbf{x}$ must have the same range-space part, which means $\mathbf{x}_{\mathcal{Y}} = \mathbf{x}^*_{\mathcal{Y}}$, and on the contrary, any vector with range-space component $\mathbf{x}^*_{\mathcal{Y}}$ satisfies the constraints of the optimization problem. Hence, the constraints uniquely determine the range-space part $\mathbf{x}^*_{\mathcal{Y}}$ of the solution, and only the $(\Pi-1)(n+1)$-dimensional part $\mathbf{x}^*_{\mathcal{Z}}$ remains unknown. This way the expected reduction in dimensionality to $(\Pi-1)(n+1)$ is performed.

To represent the null-space $\mathcal{Z}$, we use the LQ-factorization of matrix $\mathbb{A}$ [7]. Let $\mathbb{Q} \in \mathbf{R}^{\Pi(n+1)\times\Pi(n+1)}$ be an orthonormal matrix such that

$$\mathbb{AQ} = \begin{pmatrix} \mathbb{L} & 0 \end{pmatrix}, \tag{16}$$

where $\mathbb{L} \in \mathbf{R}^{(n+1)\times(n+1)}$ is a non-singular lower triangular matrix. From (16) one can see that the matrix $\mathbb{Y}$ can be chosen as the first $n+1$ columns of matrix $\mathbb{Q}$ and the matrix $\mathbb{Z}$ can be chosen as the remaining $(\Pi-1)(n+1)$ columns of $\mathbb{Q}$, i.e.

$$\mathbb{Q} = \begin{pmatrix} \mathbb{Y} & \mathbb{Z} \end{pmatrix}. \tag{17}$$

As the matrix of constraints $\mathbb{A} \in \mathbf{R}^{(n+1)\times\Pi(n+1)}$ can be written as

$$\mathbb{A} = \underbrace{(\mathbb{I}_{n+1} \quad \dots \quad \mathbb{I}_{n+1})}_{\Pi\times},$$

then the matrices $\mathbb{Y}$ and $\mathbb{Z}$ may be chosen as

$$\mathbb{Y} = \frac{1}{\sqrt{\Pi}}\mathbb{A}^T = \frac{1}{\sqrt{\Pi}} \left.\begin{pmatrix} \mathbb{I}_{n+1} \\ \mathbb{I}_{n+1} \\ \vdots \\ \mathbb{I}_{n+1} \end{pmatrix}\right\} \Pi\times,$$

$$\mathbb{Z} = \frac{1}{\sqrt{\Pi}} \underbrace{\begin{pmatrix} \mathbb{I}_{n+1} & \mathbb{I}_{n+1} & \dots & \mathbb{I}_{n+1} \\ -\mathbb{I}_{n+1} & 0 & \dots & 0 \\ 0 & -\mathbb{I}_{n+1} & & \\ \vdots & & \ddots & \\ 0 & & & -\mathbb{I}_{n+1} \end{pmatrix}}_{\Pi\times}. \tag{18}$$

For solving the constrained optimization problem we use an iterative algorithm in which a feasible initial guess $\mathbf{x}^{(0)}$ is given and the algorithm generates a sequence of feasible iterates $\mathbf{x}^{(k)}$. In every iteration, the approximation of the solution $\mathbf{x}^{(k)}$ is updated as

$$\mathbf{x}^{(k+1)} = \mathbf{x}^{(k)} + \lambda^k \mathbf{d}^{(k)}, \tag{19}$$

where $\lambda^k \in (0;1\rangle$ is the step size in the k-th iteration and $\mathbf{d}^{(k)}$ is the direction vector in the k-th iteration. We assume that $\mathbf{x}^{(k)}$ is feasible and the feasibility of $\mathbf{x}^{(k+1)}$ is required, so the direction vector $\mathbf{d}^{(k)}$ must be necessarily orthogonal to the rows of $\mathbb{A}$, i.e.

$$\mathbb{A}\mathbf{d}^{(k)} = 0, \tag{20}$$

which can be equivalently written as

$$\mathbf{d}^{(k)} = \mathbb{Z}\mathbf{d}^{(k)}_{\mathcal{Z}}, \tag{21}$$

for some $(\Pi-1)(n+1)$-dimensional vector $\mathbf{d}^{(k)}_{\mathcal{Z}}$. It can be seen that the search direction $\mathbf{d}^{(k)}$ is a $\Pi(n+1)$-dimensional vector constructed to lie in a $(\Pi-1)(n+1)$-dimensional subspace $\mathcal{Z}$. The columns of matrix $\mathbb{Z}$, which form an orthogonal basis of $\mathcal{Z}$, are given by (18), so it remains to determine the vector $\mathbf{d}^{(k)}_{\mathcal{Z}} \in \mathbf{R}^{(\Pi-1)(n+1)}$. This way the constrained minimization problem is transformed into an unconstrained problem in a lower dimension.

To find the vector $\mathbf{d}^{(k)}_{\mathcal{Z}}$, we use the modified Newton method which is based on the quadratic approximation of function ΔA around the point $\mathbf{x}^{(k)}$. Let us denote by $\mathbf{g}(\mathbf{x}) \in \mathbf{R}^{\Pi(n+1)}$ the gradient of the function ΔA which is obtained by differentiating the ΔA with respect to its variables, i.e.

$$\mathbf{g}(\mathbf{x}) = \nabla(\Delta A)^T = \begin{pmatrix} \mu_1(\mathbf{x}^*_1, T) \\ \vdots \\ \mu_n(\mathbf{x}^*_1, T) \\ -P(\mathbf{x}^*_1, T) \\ \vdots \\ \mu_1(\mathbf{x}^*_\Pi, T) \\ \vdots \\ \mu_n(\mathbf{x}^*_\Pi, T) \\ -P(\mathbf{x}^*_\Pi, T) \end{pmatrix}. \tag{22}$$

Further, let us denote by $\mathbb{H}(\mathbf{x}) \in \mathbf{R}^{\Pi(n+1)\times\Pi(n+1)}$ the Hessian of the function ΔA which is obtained by differentiating the ΔA twice with respect to its variables in a block-diagonal form with $\Pi(n+1)$ diagonal blocks given in the following form:

$$\mathbb{H}(\mathbf{x}) = \nabla^2\Delta A = \begin{pmatrix} \mathbb{H}_1 & & \\ & \ddots & \\ & & \mathbb{H}_\Pi \end{pmatrix} \quad \text{and} \quad \mathbb{H}_\alpha(\mathbf{x}) = \begin{pmatrix} \mathbb{B}^\alpha & \mathbb{C}^\alpha \\ \mathbb{C}^{\alpha T} & \mathbb{D}^\alpha \end{pmatrix}, \tag{23}$$

where $\alpha = 1, \ldots, \Pi$ and

$$\mathbb{B}^\alpha \in \mathbf{R}^{n\times n}, \quad \mathbb{B}^\alpha_{ij} = \frac{\partial \mu_i}{\partial N^*_{\alpha,j}}(\mathbf{x}^*_\alpha, T),$$
$$\mathbb{C}^\alpha \in \mathbf{R}^{n}, \quad \mathbb{C}^\alpha_{j} = -\frac{\partial P}{\partial N^*_{\alpha,j}}(\mathbf{x}^*_\alpha, T),$$
$$\mathbb{D}^\alpha \in \mathbf{R}^{1}, \quad \mathbb{D}^\alpha = -\frac{\partial P}{\partial V^*_\alpha}(\mathbf{x}^*_\alpha, T),$$

where $i, j = 1, \ldots, n$.

Approximating the function ΔA using the Taylor expansion around the point $\mathbf{x}^{(k)}$ up to the quadratic terms, the search direction $\mathbf{d}^{(k)} = \mathbb{Z}\mathbf{d}^{(k)}_{\mathcal{Z}}$ is found as a solution of the following minimization problem

$$\min_{\mathbf{d}^{(k)}\in\mathbf{R}^{\Pi(n+1)}} \Delta A(\mathbf{x}^{(k)} + \mathbf{d}^{(k)}) = \min_{\mathbf{d}^{(k)}_{\mathcal{Z}}\in\mathbf{R}^{(\Pi-1)(n+1)}} \Delta A(\mathbf{x}^{(k)} + \mathbb{Z}\mathbf{d}^{(k)}_{\mathcal{Z}}) \approx$$
$$\mathbb{A}\mathbf{d}^{(k)} = 0$$
$$\approx \min_{\mathbf{d}^{(k)}_{\mathcal{Z}}\in\mathbf{R}^{(\Pi-1)(n+1)}} \Delta A(\mathbf{x}^{(k)}) + \mathbf{g}(\mathbf{x}^{(k)})^T\mathbb{Z}\mathbf{d}^{(k)}_{\mathcal{Z}} + \frac{1}{2}(\mathbb{Z}\mathbf{d}^{(k)}_{\mathcal{Z}})^T\mathbb{H}(\mathbf{x}^{(k)})\mathbb{Z}\mathbf{d}^{(k)}_{\mathcal{Z}}. \tag{24}$$

Define a quadratic function Φ as

$$\Phi(\mathbf{d}_{\mathcal{Z}}) = \mathbf{g}(\mathbf{x}^{(k)})^T\mathbb{Z}\mathbf{d}_{\mathcal{Z}} + \frac{1}{2}\mathbf{d}^T_{\mathcal{Z}}\mathbb{Z}^T\mathbb{H}(\mathbf{x}^{(k)})\mathbb{Z}\mathbf{d}_{\mathcal{Z}},$$

then the vector $\mathbf{d}^{(k)}_{\mathcal{Z}}$ is the argument of its minimum. The function Φ has a stationary point if and only if there is a $\mathbf{d}^{(k)}_{\mathcal{Z}}$ for which the gradient of Φ vanishes, i.e.

$$\nabla\Phi(\mathbf{d}^{(k)}_{\mathcal{Z}}) = 0. \tag{25}$$

The stationary point $\mathbf{d}^{(k)}_{\mathcal{Z}}$ is a solution of the following system of equations

$$\mathbb{H}_{\mathcal{Z}}(\mathbf{x}^{(k)})\mathbf{d}^{(k)}_{\mathcal{Z}} = -\mathbf{g}_{\mathcal{Z}}(\mathbf{x}^{(k)}), \tag{26}$$

where $\mathbb{H}_{\mathcal{Z}}(\mathbf{x}^{(k)}) \in \mathbf{R}^{(\Pi-1)(n+1)\times(\Pi-1)(n+1)}$ and $\mathbf{g}_{\mathcal{Z}}(\mathbf{x}^{(k)}) \in \mathbf{R}^{(\Pi-1)(n+1)}$ are the restrictions of the Hessian matrix and of the gradient vector to the subspace $\mathcal{Z}$ defined as

$$\mathbb{H}_{\mathcal{Z}}(\mathbf{x}^{(k)}) = \mathbb{Z}^T\mathbb{H}(\mathbf{x}^{(k)})\mathbb{Z} \tag{27}$$

and

$$\mathbf{g}_{\mathcal{Z}}(\mathbf{x}^{(k)}) = \mathbb{Z}^T\mathbf{g}(\mathbf{x}^{(k)}). \tag{28}$$

Combining (18), (22), and (23), it follows from (28) that

$$\mathbf{g}_{\mathcal{Z}}(\mathbf{x}^{(k)}) = \frac{1}{\sqrt{2}}\begin{pmatrix} \mu_1(\mathbf{x}^*_1, T) - \mu_1(\mathbf{x}^*_2, T) \\ \vdots \\ \mu_n(\mathbf{x}^*_1, T) - \mu_n(\mathbf{x}^*_2, T) \\ -P(\mathbf{x}^*_1, T) + P(\mathbf{x}^*_2, T) \\ \vdots \\ \mu_1(\mathbf{x}^*_1, T) - \mu_1(\mathbf{x}^*_\Pi, T) \\ \vdots \\ \mu_n(\mathbf{x}^*_1, T) - \mu_n(\mathbf{x}^*_\Pi, T) \\ -P(\mathbf{x}^*_1, T) + P(\mathbf{x}^*_\Pi, T) \end{pmatrix}, \tag{29}$$

and from (27) that the restricted Hessian matrix can be found in the following form

$$\mathbb{H}_{\mathcal{Z}}(\mathbf{x}^{(k)}) = \frac{1}{2}\begin{pmatrix} \mathbb{H}^2_{\mathcal{Z}} & \mathbb{H}_1 & \mathbb{H}_1 \\ \mathbb{H}_1 & \ddots & \mathbb{H}_1 \\ \mathbb{H}_1 & \mathbb{H}_1 & \mathbb{H}^\Pi_{\mathcal{Z}} \end{pmatrix} \quad \text{and} \quad \mathbb{H}^\alpha_{\mathcal{Z}}(\mathbf{x}^{(k)}) = \begin{pmatrix} \widetilde{\mathbb{B}}^\alpha & \widetilde{\mathbb{C}}^\alpha \\ \widetilde{\mathbb{C}}^{\alpha T} & \widetilde{\mathbb{D}}^\alpha \end{pmatrix}, \tag{30}$$

where $\alpha = 2, \ldots, \Pi$, $\mathbb{H}_1 \in \mathbf{R}^{(n+1)\times(n+1)}$ is given by (23) and

$$\widetilde{\mathbb{B}}^\alpha \in \mathbf{R}^{n\times n}, \quad \widetilde{\mathbb{C}}^\alpha \in \mathbf{R}^{n}, \quad \widetilde{\mathbb{D}}^\alpha \in \mathbf{R}^{1},$$
$$\widetilde{\mathbb{B}}^\alpha_{ij} = \frac{\partial \mu_i}{\partial N^*_{1,j}}(\mathbf{x}^*_1, T) + \frac{\partial \mu_i}{\partial N^*_{\alpha,j}}(\mathbf{x}^*_\alpha, T),$$
$$\widetilde{\mathbb{C}}^\alpha_{j} = -\frac{\partial P}{\partial N^*_{1,j}}(\mathbf{x}^*_1, T) - \frac{\partial P}{\partial N^*_{\alpha,j}}(\mathbf{x}^*_\alpha, T)$$
$$\widetilde{\mathbb{D}}^\alpha = -\frac{\partial P}{\partial V^*_1}(\mathbf{x}^*_1, T) - \frac{\partial P}{\partial V^*_\alpha}(\mathbf{x}^*_\alpha, T),$$

where $i, j = 1, \ldots, n$. The gradient vector in (22) depends on the values of chemical potentials, which can be determined up to an arbitrary constant. Unlike in (22), the restricted gradient given by (29) is a function of differences of the chemical potentials between two states whose values can be evaluated uniquely using the equation of state.

If $\mathbf{d}^{(k)}_{\mathcal{Z}}$ solves the system of the Eq. (26) and the matrix $\mathbb{H}_{\mathcal{Z}}$ is positive definite, then the search direction $\mathbf{d}^{(k)}_{\mathcal{Z}}$ is a descent direction. If the matrix of the projected Hessian is not positive definite, then either the quadratic approximation of the function is not bounded from below, or a single minimum does not exist. In this case, it is necessary to modify the direction $\mathbf{d}^{(k)}_{\mathcal{Z}}$. If the matrix $\mathbb{H}_{\mathcal{Z}}$ is indefinite, then the vector $\mathbf{d}^{(k)}_{\mathcal{Z}}$ is found as a solution of a modified system of the equations

$$\widehat{\mathbb{H}_{\mathcal{Z}}}(\mathbf{x}^{(k)})\mathbf{d}^{(k)}_{\mathcal{Z}} = -\mathbf{g}_{\mathcal{Z}}(\mathbf{x}^{(k)}), \tag{31}$$

where $\widehat{\mathbb{H}_{\mathcal{Z}}}(\mathbf{x}^{(k)})$ is a positive definite matrix obtained by the modified Cholesky decomposition of the matrix $\mathbb{H}_{\mathcal{Z}}(\mathbf{x}^{(k)})$. In this algorithm the usual Cholesky factorization is performed to decompose matrix $\mathbb{H}_{\mathcal{Z}}(\mathbf{x}^{(k)})$ as

$$\mathbb{H}_{\mathcal{Z}}(\mathbf{x}^{(k)}) = \mathbb{L}\mathbb{D}\mathbb{L}^T,$$

where $\mathbb{L}$ is a unit lower triangular matrix and $\mathbb{D}$ is a diagonal matrix with strictly positive elements. If a negative element appears on the

diagonal of $\mathbb{D}$ during the Cholesky factorization, a suitable value is added to the corresponding diagonal element of $\mathbb{H}_{\mathcal{Z}}(\mathbf{x}^{(k)})$ to ensure positivity of matrix $\mathbb{D}$ diagonal elements in the final decomposition (see the Appendix B for details). This way we obtain the Cholesky factorization of a positive definite matrix $\widehat{\mathbb{H}_{\mathcal{Z}}}(\mathbf{x}^{(k)})$, which is used instead of matrix $\mathbb{H}_{\mathcal{Z}}(\mathbf{x}^{(k)})$ in (31) to determine the direction $\mathbf{d}_{\mathcal{Z}}^{(k)}$ in the Newton method. Due to this modification of the Newton method, the obtained direction is a descent direction. Therefore, for a sufficiently small step size $\lambda^k > 0$, the decrease of ΔA can be guaranteed. In this work, the line-search technique is used to find the step size λ^k. First, we set $\lambda^k = 1$ and test if $\Delta A(\mathbf{x}^{(k)} + \mathbf{d}^{(k)}) < \Delta A(\mathbf{x}^{(k)})$. If this condition is satisfied, we set $\mathbf{x}^{(k+1)} = \mathbf{x}^{(k)} + \mathbf{d}^{(k)}$. If not, we halve the value of λ^k until the condition $\Delta A(\mathbf{x}^{(k)} + \lambda^k \mathbf{d}^{(k)}) < \Delta A(\mathbf{x}^{(k)})$ is satisfied and then set $\mathbf{x}^{(k+1)} = \mathbf{x}^{(k)} + \lambda^k \mathbf{d}^{(k)}$. Now, a single iteration of the Newton method is completed.

The iterations are terminated when either the maximal number of iterations is achieved (500), or when a stopping criterion is satisfied and the required accuracy is achieved. In this work the stopping criterion is given by

$$\|\mathbf{d}^{(k)}\| := \left(\sum_{l=1}^{\Pi} \left(\frac{\mathbf{d}_{l(n+1)}^{(k)2}}{V^2} + \sum_{j=(l-1)(n+1)+1}^{l(n+1)-1} \frac{\mathbf{d}_j^{(k)2}}{N^2} \right) \right)^{\frac{1}{2}} \leq \varepsilon_{tol} = 10^{-10}, \tag{32}$$

where V is the total volume and N is the total number of moles. As some of the elements of the vector $\mathbf{d}^{(k)}$ have dimension mol and other m^3, the squares of the elements $\mathbf{d}_j^{(k)2}$ are weighted with the inverse square of moles and volume, respectively.

3.4. Modified Newton method for Π-Phase Split Calculation

Now we summarize the essential steps of the proposed algorithm.

Step 1 Let $N_1, \ldots, N_n$, V and $T > 0$ be given. Let Π is the number of phases. Set the number of iterations $k = 0$. Get an initial Π-phase split (initial feasible solution) $\mathbf{x}^{(0)} \in \mathbf{R}^{\Pi(n+1)}$ from the *VT*-stability algorithm as described in Section 3.2

$$\mathbf{x}^{(0)} = \begin{pmatrix} N_{1,1} \\ \vdots \\ N_{1,n} \\ V_1 \\ \vdots \\ N_{\Pi,1} \\ \vdots \\ N_{\Pi,n} \\ V_\Pi \end{pmatrix}.$$

Step 2 Assemble the Hessian matrix $\mathbb{H}_{\mathcal{Z}}(\mathbf{x}^{(k)})$ and the gradient vector $\mathbf{g}_{\mathcal{Z}}(\mathbf{x}^{(k)})$ of ΔA in the k-th iteration projected to the subspace $\mathcal{Z}$ using (30) and (29).

Step 3 Compute the projected step direction $\mathbf{d}_{\mathcal{Z}}^{(k)} \in \mathbf{R}^{(\Pi-1)(n+1)}$ and the feasible direction $\mathbf{d}^{(k)} \in \mathbf{R}^{\Pi(n+1)}$ using (26) and (21)

$$\begin{aligned} \mathbb{H}_{\mathcal{Z}}(\mathbf{x}^{(k)})\mathbf{d}_{\mathcal{Z}}^{(k)} &= -\mathbf{g}_{\mathcal{Z}}(\mathbf{x}^{(k)}), \\ \mathbf{d}^{(k)} &= \mathbb{Z}\mathbf{d}_{\mathcal{Z}}^{(k)}. \end{aligned}$$

If the matrix $\mathbb{H}_{\mathcal{Z}}(\mathbf{x}^{(k)})$ is not positive definite, find the vector $\mathbf{d}_{\mathcal{Z}}^{(k)}$ by solving a modified system of equations (31)

$$\widehat{\mathbb{H}_{\mathcal{Z}}}(\mathbf{x}^{(k)})\mathbf{d}_{\mathcal{Z}}^{(k)} = -\mathbf{g}_{\mathcal{Z}}(\mathbf{x}^{(k)}),$$

where $\widehat{\mathbb{H}_{\mathcal{Z}}}(\mathbf{x}^{(k)})$ is a positive definite matrix obtained from the modified Cholesky decomposition of matrix $\mathbb{H}_{\mathcal{Z}}(\mathbf{x}^{(k)})$.

Step 4 Determine the step length $\lambda^k > 0$ for the k-th iteration satisfying

$$\Delta A(\mathbf{x}^{(k)} + \lambda^k \mathbf{d}^{(k)}) < \Delta A(\mathbf{x}^{(k)}). \tag{33}$$

First, set the step length to $\lambda^k = 1$ and test if the condition (33) holds. If not, use the bisection method to find a value of λ^k satisfying (33).

Step 5 Update the approximation using (19)

$$\mathbf{x}^{(k+1)} = \mathbf{x}^{(k)} + \lambda^k \mathbf{d}^{(k)}.$$

Step 6 Test the convergence using (32). If needed, increase k by 1 and go to Step 2. If not needed, the algorithm ends up with the solution $\mathbf{x}^{(k+1)}$.

3.5. General strategy for Π-phase equilibria computation

In general, we do not know the number of phases a priori. Therefore, the proposed strategy is based on the repeated constant-volume stability testing and the constant-volume phase-split calculation:

Step 1 Set the number of phases $\Pi = 1$.

Step 2 Perform the Π-phase stability algorithm, which is discussed in Section 3.1 and provided in the previous work [23], to investigate whether the Π-phase state is stable or not. If it is stable, calculate the equilibrium pressure from the equation of state and the procedure ends.

Step 3 In the case the mixture is unstable, increase the number of phases Π by one and add a new phase as described in Section 3.2 to get an initial guess for the phase split calculation.

Step 4 Perform the Π-phase flash calculation to establish composition, densities and amounts of the phases using the initial guess from the stability algorithm. The numerical algorithm for the Π-phase split calculation, which is described in Section 3.3, is summarized above.

Step 5 If any of the phases disappears, i.e. $V_\alpha \to 0+$, where $\alpha \in \{1, \ldots, \Pi\}$, remove the pertinent phase and decrease Π by one. Repeat Steps 2–5 until the stability analysis decides about a stable Π-phase state.

Notice that the number of phases is changing (increasing or decreasing) during the calculation which means the number of unknows and equations to be solved is not known a priori.

4. Numerical examples of *VT*-flash calculations

We have tested the proposed strategy for Π-phase equilibrium computation on many mixtures described using the Peng–Robinson equation of state and the Cubic-Plus-Association (CPA) equation of state. In all cases the algorithm converged well and we have not found a case in which the algorithm would not converge. To demonstrate the performance of the algorithm and its robustness and efficiency, we present six examples of different level of complexity. While in Examples 1–4 the behaviour of hydrocarbon mixtures is investigated, in Examples 5 and 6 the water-containing mixtures are shown. Parameters of the

Table 1
Parameters of the Peng–Robinson and CPA equations of state for all components used in all examples (the notation is explained in Appendix A).

Component	$T_{i,crit}$ [K]	$P_{i,crit}$ [MPa]	ω_i [–]	$M_{w,i}$ [g mol^{-1}]
H_2O	647.29	22.09	0.3440	18.01528
H_2S	373.20	8.940	0.0810	34.10
CO_2	304.14	7.375	0.2390	44.0
N_2	126.21	3.390	0.0390	28.0
C_1	190.56	4.599	0.0110	16.0
C_2	305.32	4.872	0.0990	30.10
PC_1	333.91	5.329	0.1113	34.64
PC_2	456.25	3.445	0.2344	69.52
PC_3	590.76	2.376	0.4470	124.57
C_{12+}	742.58	1.341	0.9125	248.30

Peng–Robinson equation of state for all components used are presented in Table 1. Details for both equations of state used can be found in Appendix A.

In the following examples, we simulate isothermal compression of a multicomponent mixture with molar fractions $z_1, \ldots, z_n$ in a closed cell. First, the stability analysis from [23] is performed to detect the boundary between areas of different number of phases for one specific temperature or an interval of temperatures and for the whole range of feasible molar concentrations c_i. Then, the molar density c is changed at a selected temperature T and the results of the constant-volume phase-split calculations are provided for the mixture at temperature T and molar concentrations $c_i = cz_i$. At the end of the section, we present a detailed example of the phase-equilibrium computation for a ternary system from Example 3 which is unstable at given conditions. We summarize the results from the phase stability testing, providing the values of the D function, the numbers of iterations and the initial phase-split, and the results from the phase-split calculation providing both the phase properties and the equilibrium pressure as well as and the numbers of iterations and information about the line-search.

4.1. Example 1

In the first example, we investigate the phase equilibrium for a binary mixture of carbon dioxide (CO_2) and methane (C_1) with molar fractions $z_{CO_2} = 0.452587$ and $z_{C_1} = 0.547413$. The binary interaction coefficient $\delta_{CO_2\text{-}C_1} = 0.15$. First, the general phase-stability analysis at constant volume, temperature and moles is performed for temperatures $T \in \langle 180\,;260\rangle$ K and the whole range of feasible molar concentrations c. In Fig. 1 (left) we can see the approximate boundary between the single-phase, two-phase and three-phase areas in the c, T-space. As shown in Fig. 1 (left), when compressing at temperature $T = 205$ K, the mixture occurs in single-phase for the lowest molar concentrations, then becomes two-phase for molar concentrations up to approximately 12 kmol m^{-3}. Then the mixture becomes three-phase, while at molar concentrations higher than 18 kmol m^{-3} becomes two-phase again. For molar concentrations between 25 kmol m^{-3} and 35 kmol m^{-3} the mixture occurs in single-phase and for the highest molar concentrations becomes two-phase again.

In Fig. 2, volume fractions and mass densities of each phase are presented as functions of the molar density c. In Fig. 3, molar fractions of both components in each phase can be seen as functions of the molar density c. In Fig. 1 (right), the equilibrium pressure is presented as a function of the molar density c illustrating a steady rise of the equilibrium pressure during the compression in two-phase, followed by the constant value of pressure within the three-phase area (for molar concentrations between approximately 12 kmol m^{-3} and 18 kmol m^{-3}) and the substantial increase in pressure at molar concentrations higher than 18 kmol m^{-3} when all gas is depleted. Notice that as the pressure is constant during the compression in the three-phase region, the mass densities of each phase and the composition of each phase remain constant as well.

In Fig. 1 (right), the pressure in the three-phase domain is constant, demonstrating the similar behaviour as pure components at saturation pressure. For this value of pressure P, temperature T, and mole numbers N, the volume of the system is ambiguous. In contrast, when we specify V, T, N, the pressure P is determined uniquely. This is an advantageous feature of the VT-flash. When PT-flash is used in a compositional simulator, the ambiguity of volume in the PT-formulation generally leads to breakdown of the computation (see [30]). The VT-flash does not suffer from this issue.

Note that we can observe the second two-phase region for high molar concentrations c and low temperatures T corresponding to a liquid–liquid two-phase area as can be seen from the values of mass densities of the phases (see Fig. 2).

4.2. Example 2

In the second example, we investigate the phase equilibrium for a binary mixture of nitrogen (N_2) and ethane (C_2) with molar fractions $z_{N_2} = 0.547413$ and $z_{C_2} = 0.452587$. The binary interaction coefficient $\delta_{N_2\text{-}C_2} = 0.08$. First, the general phase-stability analysis at constant volume, temperature and moles is performed for temperatures $T \in \langle 120\,;280\rangle$ K and the whole range of feasible

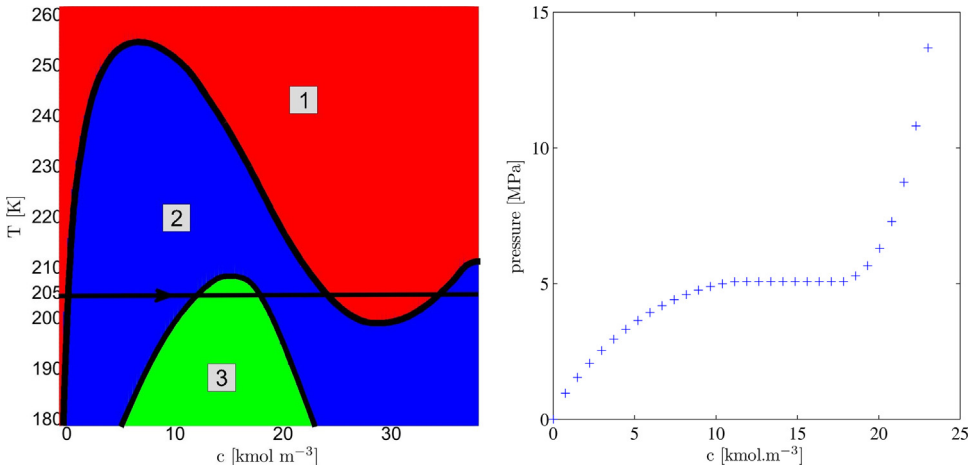

Fig. 1. Approximate boundary between the single-phase, two-phase and three-phase regions in the c, T-space (left). Equilibrium pressure as a function of the molar density c at $T = 205$ K (right). Example 1: binary CO_2–C_1 mixture.

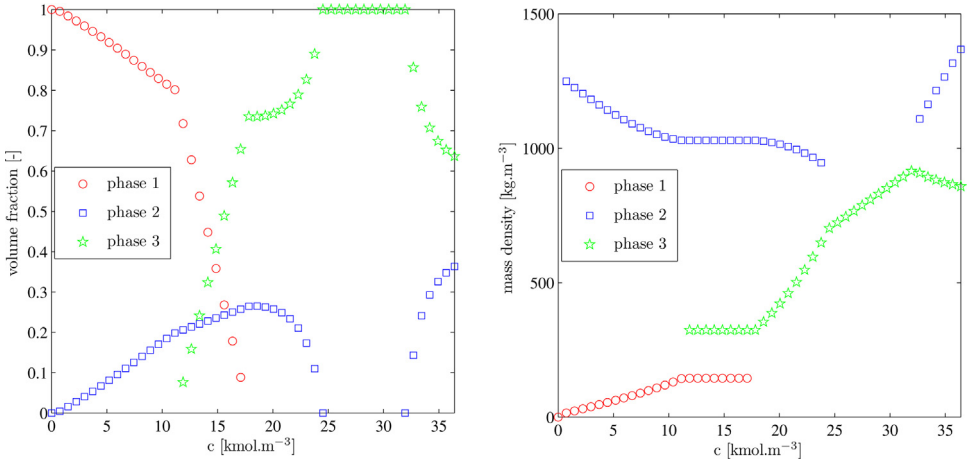

Fig. 2. Volume fractions (left) and mass densities (right) of each phase as functions of the molar density c at $T = 205$ K. Example 1: binary CO_2–C_1 mixture.

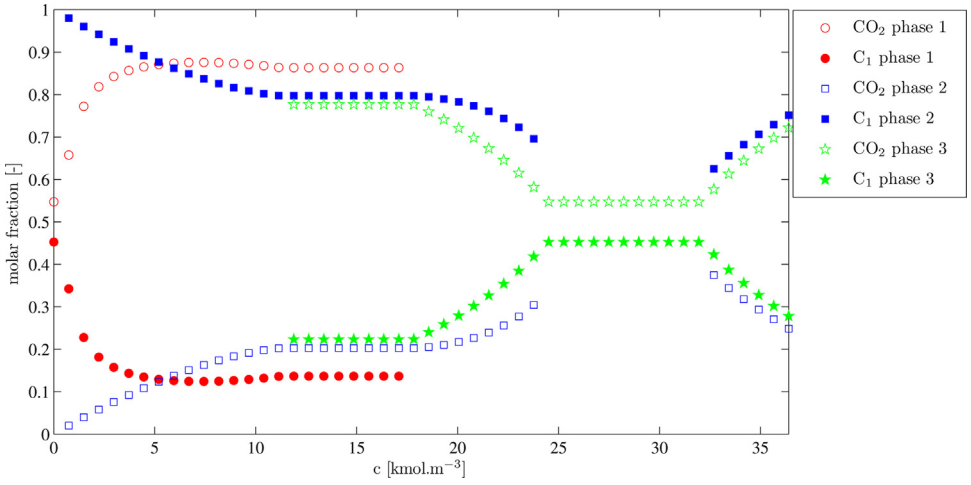

Fig. 3. Molar fractions of both components in each phase as functions of the molar density c at $T = 205$ K. Example 1: binary CO_2–C_1 mixture.

molar concentrations c. In Fig. 4 (left) we can see the approximate boundary between the single-phase, two-phase and three-phase areas in the c, T-space. As shown in Fig. 4 (left), when compressing at extremely low temperature $T = 125$ K, the mixture occurs in single-phase for the lowest molar concentrations, then becomes two-phase, while at molar concentrations higher than 10 kmol m^{-3} the mixture becomes three-phase. For molar concentrations higher than approximately 20 kmol m^{-3} the mixture occurs in two-phase again.

In Fig. 5, volume fractions of each phase and mass densities of each phase are presented as functions of the molar density c. Note that the mass densities of both phases in the two-phase region intersect at molar concentration approximately 25 kmol m^{-3} and switch, i.e. the heavier phase becomes the lighter one and the

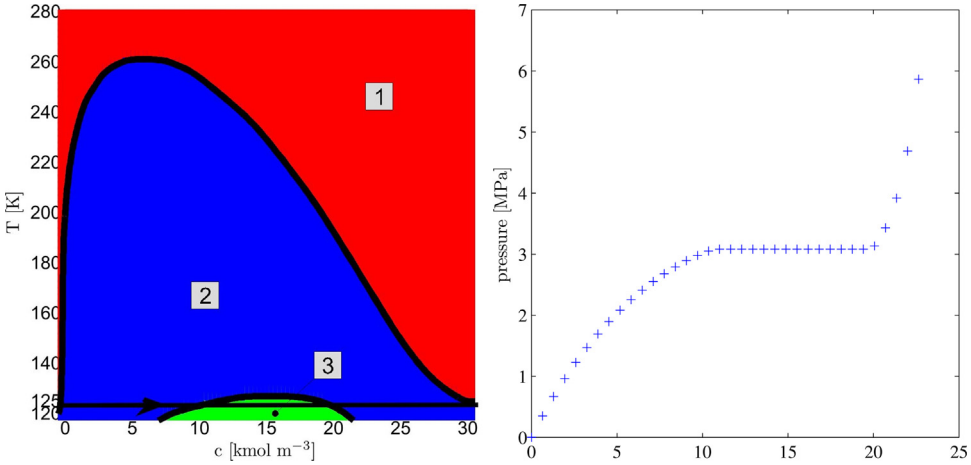

Fig. 4. Approximate boundary between the single-phase, two-phase and three-phase regions in the c, T-space (left). Equilibrium pressure as a function of the molar density c at $T = 125$ K (right). Example 2: binary N_2–C_2 mixture.

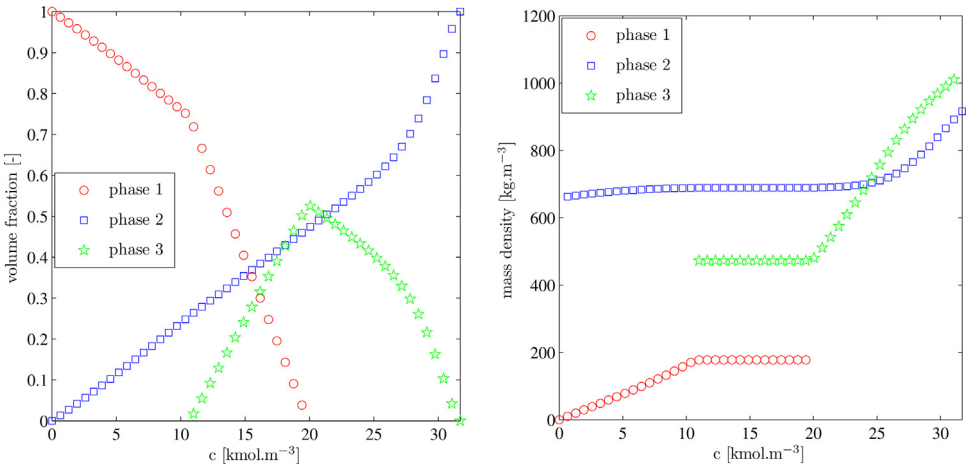

Fig. 5. Volume fractions (left) and mass densities (right) of each phase as functions of the molar density c at $T = 125$ K. Example 2: binary N_2–C_2 mixture.

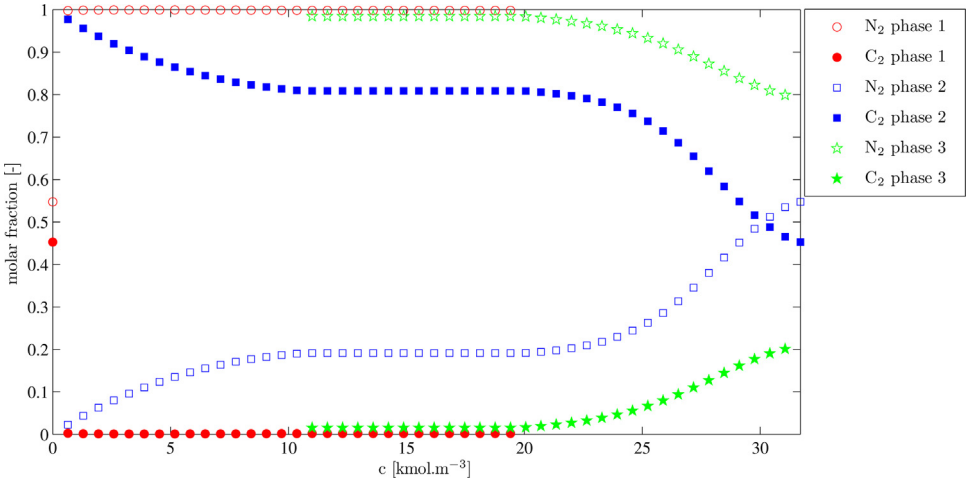

Fig. 6. Molar fractions of both components in each phase as functions of the molar density c at $T = 125$ K. Example 2: binary N_2–C_2 mixture.

lighter phase becomes the heavier one. Molar fractions of both components in each phase are presented as functions of the molar density c in Fig. 6. In Fig. 4 (right), the equilibrium pressure is presented as a function of the molar density c illustrating a steady rise of the equilibrium pressure during the compression in two-phase area, followed by the constant value of pressure within the three-phase area (for molar concentrations between approximately 10 kmol m^{-3} and 20 kmol m^{-3}), demonstrating the similar behaviour as pure components at saturation pressure, and the substantial increase in pressure at molar concentrations higher than 20 kmol m^{-3} when the gas phase is depleted. Notice that as the pressure is constant during the compression in the three-phase region, the mass densities of each phase and the composition of each phase remain constant as well.

Note that while at lower molar concentrations c and low temperatures T the two-phase region corresponds to a gas–liquid two-phase region, at high molar concentrations c and low temperatures T we can observe the second two-phase area corresponding to a liquid–liquid two-phase region as can be seen from the values of mass densities of the phases (see Fig. 5).

4.3. Example 3

In the third example, we investigate the phase equilibrium for a ternary mixture of hydrogen disulfide (H_2S), carbon dioxide (CO_2) and methane (C_1) with molar fractions $z_{H_2S} = 0.4989$, $z_{CO_2} = 0.0988$ and $z_{C_1} = 0.4023$. The binary interaction coefficients are presented in Table 2. First, the general phase-stability analysis at constant volume, temperature and moles is performed for temperatures $T \in \langle 100\,;350\rangle$ K and the whole range of feasible molar concentrations c. In Fig. 7 we can see the approximate boundary between the single-phase, two-phase, three-phase and even four-phase areas in the c, T-space. When compressing at extremely low temperature $T = 150$ K (see the arrow A in Fig. 7), the mixture occurs in single-phase for the lowest molar concentrations, then becomes two-phase for molar concentrations up to approximately 2 kmol m^{-3}, while for the molar concentrations up to 30 kmol m^{-3} occurs in three-phase. At higher molar concentrations the mixture becomes two-phase again. When compressing at even lower temperature $T = 130$ K (see the arrow B in Fig. 7), the mixture occurs in two-phase and three-phase for the lowest molar concentrations, then becomes four-phase for molar concentrations up to approximately 30 kmol m^{-3}, while at higher molar concentrations occurs in three-phase again.

Table 2
Binary interaction coefficients for the ternary mixture used in Example 3.

Component	H_2S	CO_2	C_1
H_2S	0	0.097	0.095
CO_2	0.097	0	0.130
C_1	0.095	0.130	0

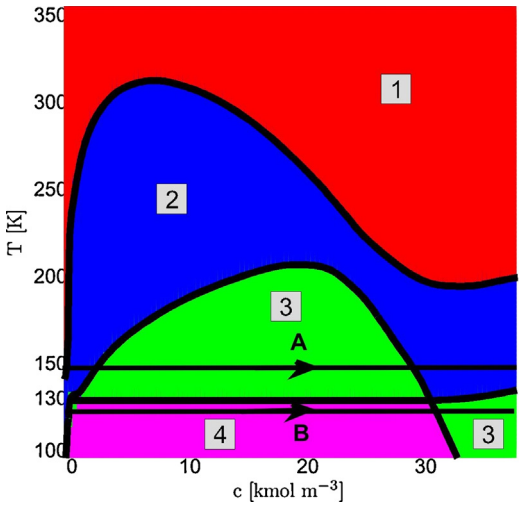

Fig. 7. Approximate boundary between the single-phase, two-phase, three-phase and four-phase regions in the c, T-space. Example 3: ternary H_2S–CO_2–C_1 mixture.

In Figs. 9 and 10, volume fractions of each phase and mass densities of each phase are presented as functions of the molar density c for both temperatures $T = 150$ K and $T = 130$ K, respectively. We do not present the plots of molar fractions of each component in each phase as functions of the molar density c which suffers from the lack of clarity in three- and more component mixtures. In Fig. 8 (right), the equilibrium pressure is presented as a function of the molar density c for temperature $T = 130$ K illustrating a steady rise of the equilibrium pressure during the compression, followed by the constant value of pressure within the four-phase area (for molar concentrations between approximately 0.1 kmol m^{-3} and 30 kmol m^{-3}) demonstrating the similar behaviour as pure components at saturation pressure, and the substantial increase at molar concentrations higher than 30 kmol m^{-3} when the gas phase is depleted. Similarly, the same is presented at temperature $T = 130$ K in Fig. 8 (left) in which the equilibrium pressure within the three-phase area seems to be constant but it is not exactly constant; there is a very slow increase from 0.995166 MPa for molar concentration of 10 kmol m^{-3} to 0.997523 MPa for molar concentration of 20 kmol m^{-3}. In this situation for each pressure P within this range there is a unique volume of the system V, however, volume V is very sensitive to small changes of the pressure P. This sensitivity can cause numerical difficulties in compositional transport simulation if the flash equilibrium is computed using the conventional

Table 3
Binary interaction coefficients for the reservoir fluid used in Example 4.

Component	N_2	CO_2	C_1	PC_1	PC_2	PC_3	C_{12+}
N_2	0.000	0.000	0.100	0.100	0.100	0.100	0.100
CO_2	0.000	0.000	0.150	0.150	0.150	0.150	0.150
C_1	0.100	0.150	0.000	0.035	0.040	0.049	0.069
PC_1	0.100	0.150	0.035	0.000	0.000	0.000	0.000
PC_2	0.100	0.150	0.040	0.000	0.000	0.000	0.000
PC_3	0.100	0.150	0.049	0.000	0.000	0.000	0.000
C_{12+}	0.100	0.150	0.069	0.000	0.000	0.000	0.000

PT-flash methods. Compositional simulators using the *VT*-flash do not suffer from this issue, see [30].

Notice that as the pressure is constant and almost constant during the compression in the four-phase and three-phase regions, respectively, the mass densities of each phase and the composition of each phase remain constant or almost constant as well.

4.4. Example 4

In the fourth example, we investigate the phase equilibrium for a seven-component mixture of a multicomponent oil mixed with carbon dioxide (CO_2). The oil is modeled by seven (pseudo)components – N_2, CO_2, methane (C_1), and four hydrocarbon pseudo-components denoted as PC_1 ($H_2S + C_2 + C_3$), PC_2 (C_4–C_6), PC_3 (C_7–C_{11}), and C_{12+}. In this example oil is mixed with CO_2 to obtain a CO_2-rich seven-component mixture with molar fractions $z_{N_2} = 0.000131$, $z_{CO_2} = 0.568185$, $z_{C_1} = 0.246739$, $z_{PC_1} = 0.086275$, $z_{PC_2} = 0.033722$, $z_{PC_3} = 0.037006$ and $z_{C_{12+}} = 0.027941$. The binary interaction coefficients are shown in Table 3. First, the *VT*-stability analysis is performed for temperatures $T \in \langle 250\,;\,650 \rangle$ K and the whole range of feasible molar concentrations c. In Fig. 11 (left) we can see the approximate boundary between the single-phase, two-phase and three-phase areas in the c, T-space. As shown in Fig. 11 (left), when compressing at temperature $T = 260$ K, the mixture occurs in two-phase from the lowest molar concentrations up to approximately 0.4 kmol m^{-3}, then becomes three-phase, while at molar concentrations higher than 14 kmol m^{-3} the mixture becomes two-phase again.

In Fig. 12, volume fractions of each phase and mass densities of each phase are presented as functions of the molar density c. Note that the mass densities of a pair of phases intersect even twice, first in the three-phase area, at molar concentration approximately 10 kmol m^{-3}, and second in the two-phase area, at molar concentration approximately 15 kmol m^{-3}, and switch, i.e. the heavier phase becomes the lighter one and the lighter phase

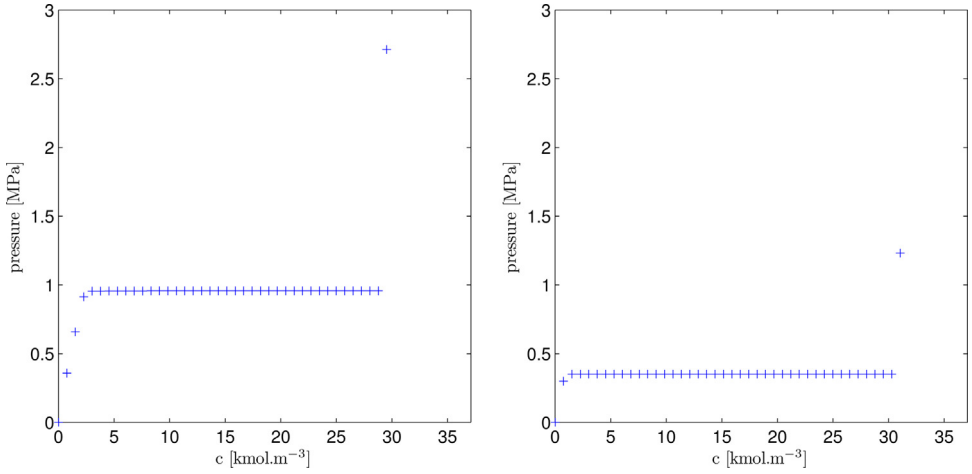

Fig. 8. Equilibrium pressures as functions of the molar density c at $T = 150$ K (left) and $T = 130$ K (right). Example 3: ternary H_2S–CO_2–C_1 mixture.

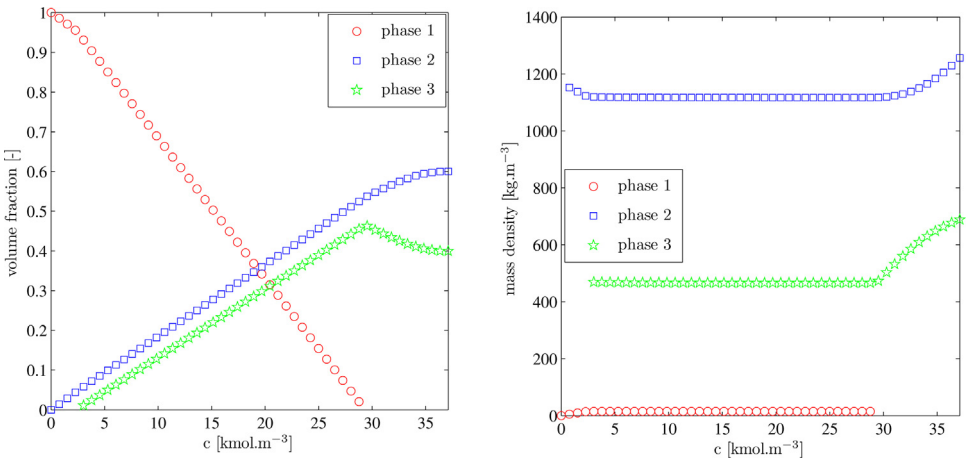

Fig. 9. Volume fractions (left) and mass densities (right) of each phase as functions of the molar density c at $T = 150$ K. Example 3: ternary H_2S–CO_2–C_1 mixture.

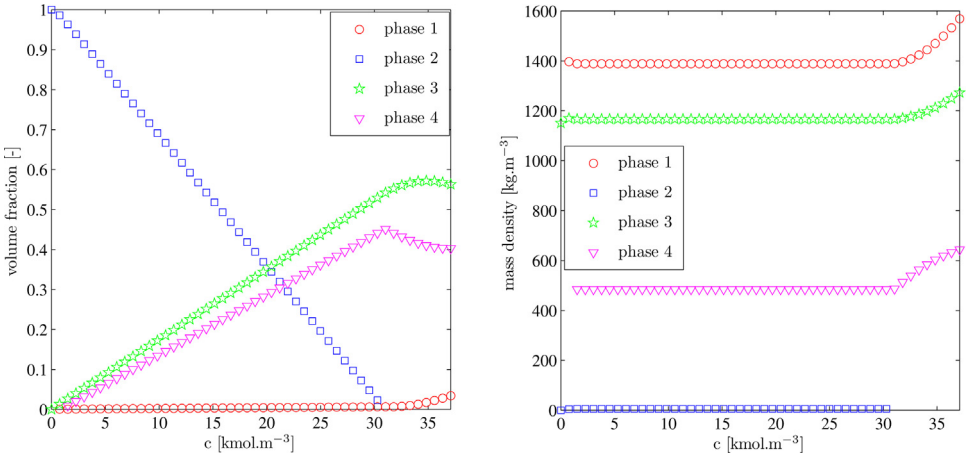

Fig. 10. Volume fractions (left) and mass densities (right) of each phase as functions of the molar density c at $T = 130$ K. Example 3: ternary H_2S–CO_2–C_1 mixture.

becomes the heavier one. We do not present the plot of molar fractions of each component in each phase as functions of the molar density c which suffers from the lack of clarity in multi-component mixtures. In Fig. 11 (right), the equilibrium pressure is presented as a function of the molar density c illustrating a steady rise of the equilibrium pressure during the compression in two-phase and three-phase, and its substantial increase at molar concentrations 14 kmol m^{-3} and higher when the gas phase is depleted.

Note that while at lower molar concentrations c and low temperatures T the two-phase region corresponds to a gas–liquid two-phase region, at high molar concentrations c and low

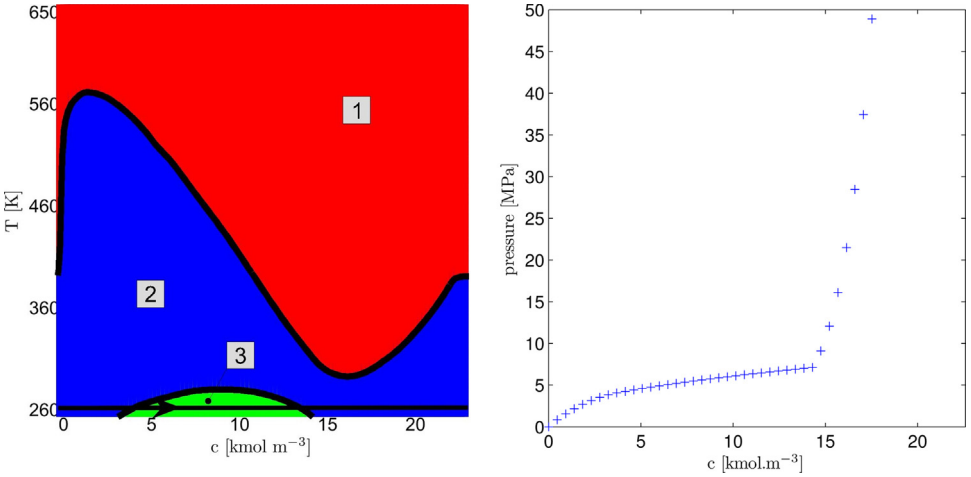

Fig. 11. Approximate boundary between the single-phase, two-phase and three-phase regions in the c, T-space (left). Equilibrium pressure as a function of the molar density c at $T = 260$ K (right). Example 4: seven-component mixture rich in CO_2.

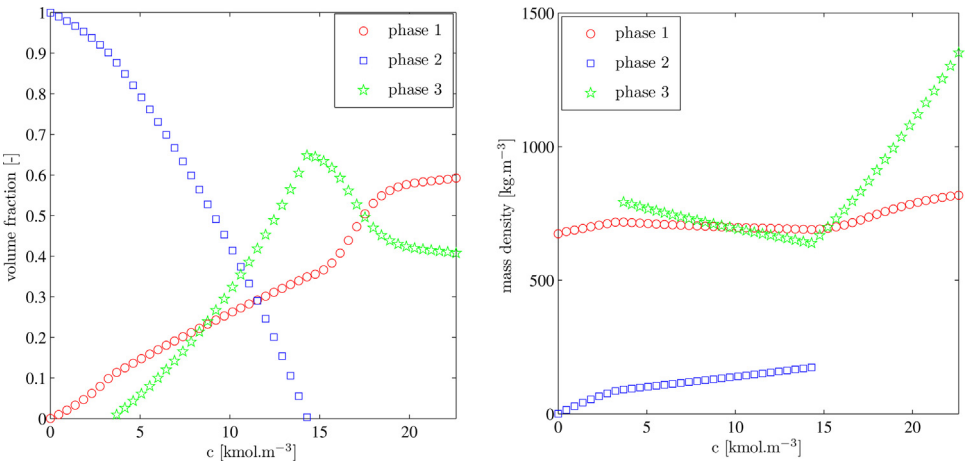

Fig. 12. Volume fractions (left) and mass densities (right) of each phase as functions of the molar density c at $T = 260$ K. Example 4: seven-component mixture rich in CO_2.

temperatures T we can observe the second two-phase area corresponding to a liquid–liquid two-phase region as can be seen from the values of mass densities (see Fig. 12).

4.5. Example 5

In the fifth example, we investigate the phase equilibrium for a binary mixture of water (H_2O) and carbon dioxide (CO_2) with molar fractions $z_{H_2O} = 0.5$ and $z_{CO_2} = 0.5$ at temperature $T = 290.15$ K. The binary interaction coefficient $\delta_{H_2O\text{–}CO_2} = 0.063028467$. The cross association factor used in the CPA equation of state for temperature T is $s_{CO_2} = 0.017386941$.

As can be seen in Figs. 13 and 14, when compressing the mixture at temperature $T = 290.15$ K, the mixture occurs in two-phase from the lowest molar concentrations up to approximately 0.7 kmol m^{-3}, then becomes three-phase, while at molar concentrations higher than 26 kmol m^{-3} the mixture becomes two-phase again.

In Fig. 13, volume fractions of each phase and mass densities of each phase are presented as functions of the molar density c. Note that the mass densities of both phases intersect in the two-phase region at molar concentration approximately 34 kmol m^{-3} and switch, i.e. the heavier phase becomes the lighter one and the lighter phase becomes the heavier one. Molar fractions of each component in each phase are presented as functions of the molar density c in Fig. 14 in which the limited mutual solubility of CO_2 and water can be seen. In Fig. 15, the equilibrium pressure is presented as a function of the molar density c illustrating a steady rise of the equilibrium pressure during the compression in two-phase area, followed by the constant value of pressure within the three-phase area (for molar concentrations between approximately 0.7 kmol m^{-3} and 26 kmol m^{-3}), demonstrating the similar behaviour as pure components at saturation pressure, and the substantial increase at molar concentrations higher than 26 kmol m^{-3} when the gas phase is depleted. Notice again that as the pressure is constant during the compression in the three-phase region, the mass densities of each phase and the composition of each phase remain constant as well.

Note that while at lower molar concentrations c and low temperatures T the two-phase region corresponds to a gas–liquid two-phase region, at high molar concentrations c and low temperatures T we can observe the second two-phase area corresponding to a liquid–liquid two-phase region as can be seen from the values of mass densities of the phases (see Fig. 13).

4.6. Example 6

In the sixth example, we investigate the phase equilibrium for a four-component mixture of water (H_2O), hydrogen disulfide (H_2S), carbon dioxide (CO_2) and methane (C_1) with molar fractions $z_{H_2O} = 0.5008$, $z_{H_2S} = 0.3986$, $z_{CO_2} = 0.0502$ and $z_{C_1} = 0.0504$ at temperature $T = 310.95$ K. The binary interaction coefficients are presented in Table 4. The cross association factors used in the CPA equation of state for temperature T are $s_{H_2S} = 0.038322796$, $s_{CO_2} = 0.026637098$ and $s_{C_1} = 0.0$.

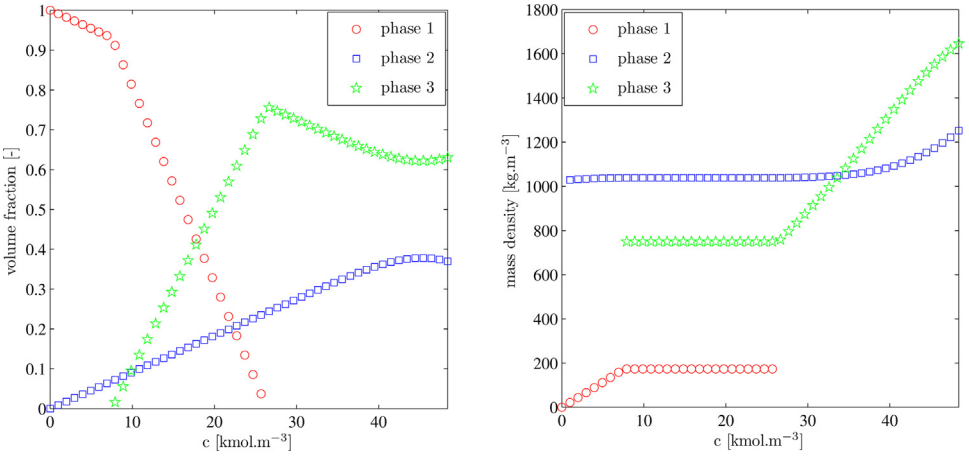

Fig. 13. Volume fractions (left) and mass densities (right) of each phase as functions of the molar density c at $T = 290.15$ K. Example 5: binary H_2O–CO_2 mixture.

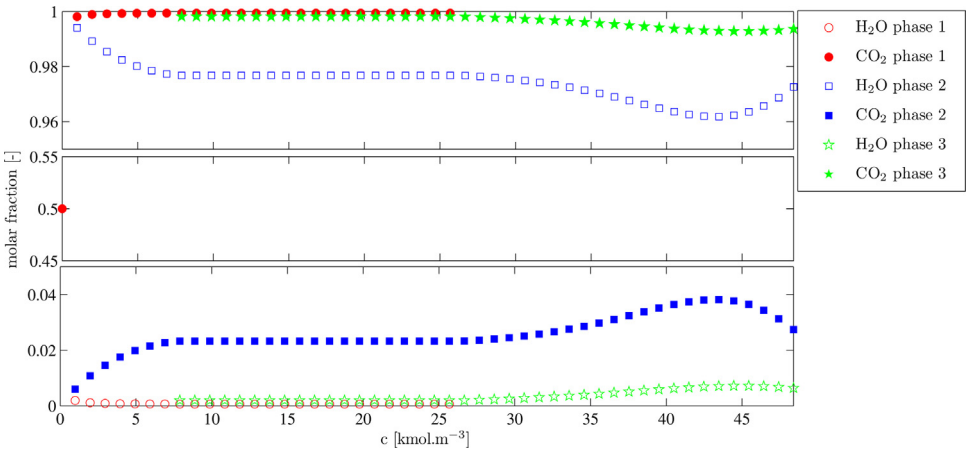

Fig. 14. Molar fractions of both components in each phase as functions of the molar density c at $T = 290.15$ K. Example 5: binary H_2O–CO_2 mixture.

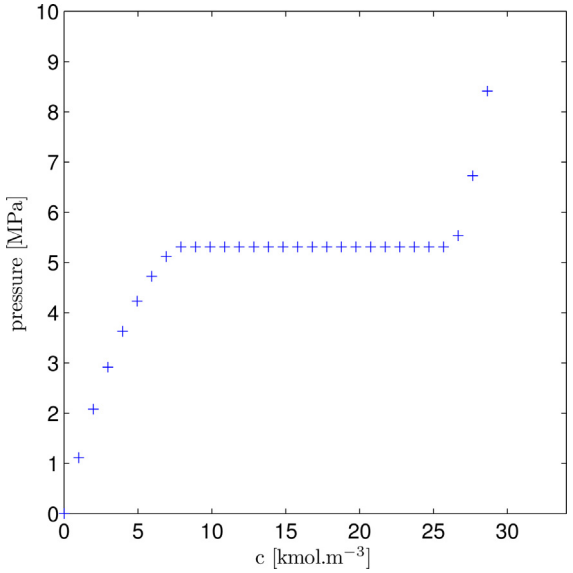

Fig. 15. Equilibrium pressure as a function of the molar density c at $T = 290.15$ K. Example 5: binary H_2O–CO_2 mixture.

Table 4
Binary interaction coefficients for the four-component mixture used in Example 6.

Component	H_2O	H_2S	CO_2	C_1
H_2O	0	0.13862	0.10402	0.06802
H_2S	0.13862	0	0	0.100
CO_2	0.10402	0	0	0.150
C_1	0.06802	0.100	0.150	0

As can be seen in Fig. 16, when compressing the mixture at temperature $T = 310.95$ K, the mixture occurs in two-phase from the lowest molar concentrations up to approximately 0.3 kmol m^{-3}, then becomes three-phase, while at molar concentrations higher than 30 kmol m^{-3} the mixture becomes two-phase again.

In Fig. 16, volume fractions of each phase and mass densities of each phase are presented as functions of the molar density c. Note that the mass densities of both phases intersect in the two-phase region at molar concentration approximately 42 kmol m^{-3} and attain the same value for higher molar concentrations. We do not present the plot of molar fractions of each component in each phase as functions of the molar density c which suffers from the lack of clarity in multicomponent mixtures. In Fig. 17, the equilibrium pressure is presented as a function of the molar density c illustrating a steady rise of the equilibrium pressure during the compression in two-phase and three-phase area, and its substantial increase at molar concentrations higher than 30 kmol m^{-3} when the gas phase is depleted.

Note that while at lower molar concentrations c and low temperatures T the two-phase region corresponds to a gas–liquid two-phase region, at high molar concentrations c and low temperatures T we can observe the second two-phase area corresponding

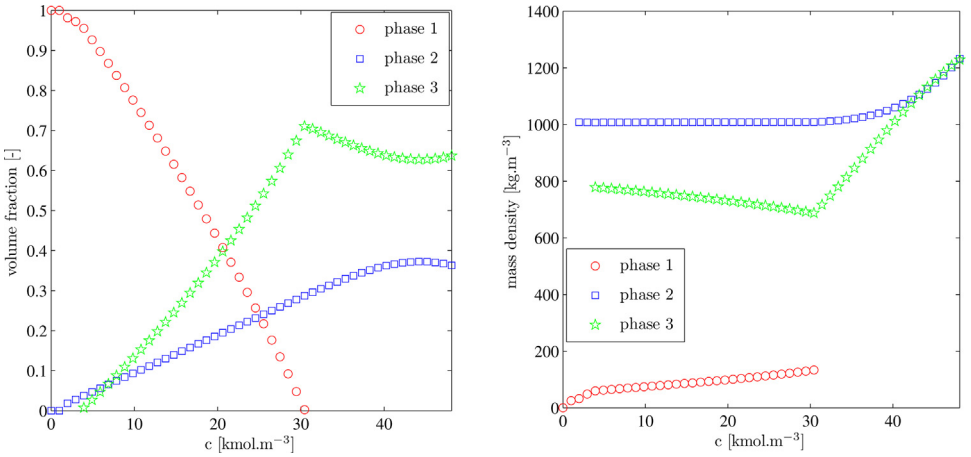

Fig. 16. Volume fractions (left) and mass densities (right) of each phase as functions of the molar density c at $T = 310.95$ K. Example 6: four-component H_2O–H_2S–CO_2–C_1 mixture.

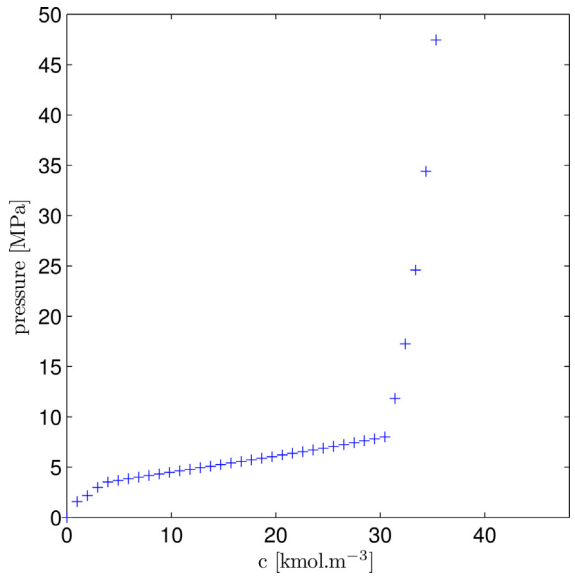

Fig. 17. Equilibrium pressure as a function of the molar density c at $T = 310.95$ K. Example 6: four-component H_2O–H_2S–CO_2–C_1 mixture.

Table 5
Parameters of the CPA equation of state for Examples 5 and 6 (the notation is explained in Appendix A).

Symbol	Units	Value
$\kappa^{\alpha\beta}$	[m^{3}mol^{-1}]	$1.80151 \cdot 10^{-6}$
$\epsilon^{\alpha\beta}/k_B$	[K]	1738.39360
c_0	[J m^{-3} mol^{-2}]	0.09627
c_1	[–]	1.75573
c_2	[–]	0.00352
c_3	[–]	−0.27464

Table 6
The change in the total Helmholtz energy in each iteration in the first two-phase flash at constant temperature $T = 170.2$ K and volume for a ternary mixture of H_2S–CO_2–C_1.

Iteration	Change in energy
1	−23,372.8
2	−8,594.3
3	−2,031.7
4	−204.7
5	−3.78
6	−0.002
7	$-4.4 \cdot 10^{-8}$
8	$-5.6 \cdot 10^{-8}$

to a liquid–liquid two-phase region as can be seen from the values of mass densities of the phases (see Fig. 16).

4.7. Detailed example of phase-equilibrium computation

To give a detailed example of the Π-phase equilibrium computation using the general strategy, we investigate the phase equilibrium for a ternary mixture of hydrogen disulfide (H_2S), carbon dioxide (CO_2) and methane (C_1) of total molar concentration $c = 28.02$ kmol m^{-3} with molar fractions $z_{H_2S} = 0.4989$, $z_{CO_2} = 0.0988$ and $z_{C_1} = 0.4023$ at temperature $T = 170.2$ K. Parameters of the Peng–Robinson equation of state for all components used are presented in Table 1 and the binary interaction coefficients are presented in Table 2.

Set the number of phases $\Pi = 1$. Performing the single-phase stability algorithm on the overall mixture, we obtain a negative value of the D function $\left(D_{\min} = -2.02265 \cdot 10^7 \text{ Pa}\right)$; the mixture is unstable. Note that we use several initial guesses in the modified Newton algorithm, thereby we get several values of the D function from which the minimal value is taken to determine whether the mixture is stable or not. The result is achieved in 6 iterations, no line-search is needed.

As the mixture is unstable, the stability algorithm provides us a trial phase with the following molar concentrations of each component:

$$c'_{H_2S} = 5.23239 \text{ mol m}^{-3},$$
$$c'_{CO_2} = 6.72906 \text{ mol m}^{-3},$$
$$c'_{C_1} = 908.086 \text{ mol m}^{-3}.$$

The volume fraction of the trial phase S' is found to satisfy the restrictions (11) and (12) as S'=0.1998. For the other phase the molar concentrations of each component and the volume fraction are computed from (10). The value of the trial phase volume fraction is reduced using the bisection method such that $\Delta A = A^{II} - A^{I} < 0$, where A^I and A^{II} are the single-phase and two-phase states, respectively, and an initial phase-split with the following properties is obtained for the two-phase split calculation such that $\Delta A = -538314$ J

$$c'_{H_2S} = 5.23239 \text{ mol m}^{-3}, \quad c''_{H_2S} = 14713.9 \text{ mol m}^{-3},$$
$$c'_{CO_2} = 6.72906 \text{ mol m}^{-3}, \quad c''_{CO_2} = 2913.57 \text{ mol m}^{-3},$$
$$c'_{C_1} = 908.086 \text{ mol m}^{-3}, \quad c''_{C_1} = 11817.4 \text{ mol m}^{-3},$$
$$S' = 0.04995, \quad S'' = 0.95005.$$

Increase the number of phases to $\Pi = 2$. Performing the two-phase split calculation, an equilibrium two-phase state is found in 8 iterations, no line-search is needed. The change in the total Helmholtz energy in each iteration is presented in Table 6. The resulting phase properties are summarized in Table 7. The total change in the Helmholtz energy with respect to the initial single-phase state is $\Delta A = -572521.4$ J.

Performing the single-phase stability algorithm on one of two equilibrium phases, we obtain a negative value of the D function $\left(D_{\min} = -4.1226 \cdot 10^6 \text{ Pa}\right)$; the mixture is unstable. The result is achieved in 8 iterations, no line-search is needed. Further, the stability algorithm provides us a trial phase with the following molar concentrations of each component

$$c'_{H_2S} = 1773.55 \text{ mol m}^{-3},$$
$$c'_{CO_2} = 864.69 \text{ mol m}^{-3},$$
$$c'_{C_1} = 21149.20 \text{ mol m}^{-3}.$$

The volume fraction of the trial phase S' is found to satisfy the restrictions (11) and (12) as S'=0.001307. For the other two phases the molar concentrations of each component and the volume fractions are computed from (10). The value of the trial phase volume fraction is reduced using the bisection method such that $\Delta A = A^{III} - A^{II} < 0$, where A^{II} and A^{III} are the two-phase and three-phase states, respectively. The initial phase-split with the following

Table 7
Overall properties of the ternary mixture of H_2S–CO_2–C_1 and resulting phase properties in the first two-phase flash at constant temperature $T = 170.2$ K and volume. The resulting equilibrium pressure is $P = 26.59$ bar.

Property	Unit	Overall mixture	Phase 1	Phase 2
Molar density	[mol m^{-3}]	28,020.0	3,261.02	29,451.0
Molar fraction of H_2S	[–]	0.4989	0.006514	0.502051
Molar fraction of CO_2	[–]	0.0988	0.007875	0.099382
Molar fraction of C_1	[–]	0.4023	0.985611	0.398567
Phase volume fraction	[–]		0.054640	0.945360
Mass density	[kg m^{-3}]		53.41	820.97

Table 8
The change in the total Helmholtz energy in each iteration in the second two-phase flash at constant temperature $T = 170.2$ K and volume for the ternary mixture of H_2S–CO_2–C_1.

Iteration	Change in energy
1	−48,169.1
2	−103,222.4
3	−8,328.5
4	−104.5
5	−0.02
6	$-4.5 \cdot 10^{-8}$
7	$-6.3 \cdot 10^{-9}$

properties is obtained for the three-phase split calculation such that $\Delta A = -3660.5$ J

$$c'_{H_2S} = 1773.55 \text{ mol m}^{-3}, \quad c''_{H_2S} = 0.2150 \text{ mol m}^{-3}, \quad c'''_{H_2S} = 14794.917 \text{ mol m}^{-3},$$
$$c'_{CO_2} = 864.69 \text{ mol m}^{-3}, \quad c''_{CO_2} = 15.521 \text{ mol m}^{-3}, \quad c'''_{CO_2} = 2928.324 \text{ mol m}^{-3},$$
$$c'_{C_1} = 21149.20 \text{ mol m}^{-3}, \quad c''_{C_1} = 2996.913 \text{ mol m}^{-3}, \quad c'''_{C_1} = 11731.687 \text{ mol m}^{-3},$$
$$S' = 0.001307, \quad S'' = 0.053986, \quad S''' = 0.944707.$$

Increase the number of phases to $\Pi = 3$. Performing the three-phase split calculation, we observe that in 24 iterations one of the three phases disappears, i.e. its volume fraction is lower than 1.10^{-9}. Therefore, the pertinent phase is removed and an initial two-phase split is obtained as

$$c'_{H_2S} = 1664.420 \text{ mol m}^{-3}, \quad c''_{H_2S} = 22428.651 \text{ mol m}^{-3},$$
$$c'_{CO_2} = 1014.645 \text{ mol m}^{-3}, \quad c''_{CO_2} = 3971.652 \text{ mol m}^{-3},$$
$$c'_{C_1} = 20815.986 \text{ mol m}^{-3}, \quad c''_{C_1} = 4724.376,$$
$$S' = 0.406924, \quad S'' = 0.593076.$$

The total change in the Helmholtz energy with respect to the initial single-phase state is $\Delta A = -2222386.2$ J.

The number of phases is decreased by one to $\Pi = 2$. Performing the two-phase split calculation, an equilibrium two-phase state, which is different from the previous one obtained from the two-phase flash (see Table 7 and 10), is found in 7 iterations. Note that no line-search is needed in any iteration. The change in the total Helmholtz energy in each iteration is presented in Table 8. The resulting phase properties are summarized in Table 9. The total change in the Helmholtz energy with respect to the initial single-phase state is $\Delta A = -2382210.7$ J.

Performing the single-phase stability algorithm on one of two equilibrium phases, we obtain a positive value of the D function; the two-phase state is stable and the equilibrium pressure is $P = 52.78$ bar.

To summarize, both the increase and decrease in the number of phases are observed in this example demonstrating that passing through the region with higher number of phases (three-phase region in this case) enables leaving the local minimum and moving to a state with lower both the number of phases and energy (two-phase state in this case), i.e. the global minimum.

In all cases, the number of iterations were similar to those in the detailed example regardless the number of components. Furthermore, quadratic convergence of the Newton–Raphson method has been observed. Thus, numerical errors can be estimated from the size of increment in the last few iterations [31]. Using the Euclidean norm, the estimated error is approximately 10^{-14}.

5. Discussion and conclusions

We have extended the results of our previous work, in which we have dealt with the single-phase stability testing and two-phase split calculation in a multicomponent mixture in a closed cell, both at constant volume, temperature and moles, to a general strategy for Π-phase split calculation at constant volume, temperature and moles, where $\Pi \in N$ is the number of phases. As the number of phases is not necessarily known a priori, the proposed strategy is based on the repeated constant-volume stability testing and constant-volume phase-split calculation until a stable Π-phase state is found. The proposed strategy has been tested on many mixtures of different level of complexity under different conditions including hydrocarbon mixtures and water-containing mixtures described by the Cubic-Plus-Association equation of state.

Table 9
Overall properties of the ternary mixture of H_2S–CO_2–C_1 and resulting phase properties in the second two-phase flash at constant temperature $T = 170.2$ K and volume. The resulting equilibrium pressure is $P = 52.78$ bar.

Property	Unit	Overall mixture	Phase 1	Phase 2
Molar density	[mol m^{-3}]	28,020.0	23,978.19	31,557.58
Molar fraction of H_2S	[–]	0.4989	0.086673	0.773045
Molar fraction of CO_2	[–]	0.0988	0.062169	0.123161
Molar fraction of C_1	[–]	0.4023	0.851158	0.103794
Phase volume fraction	[–]		0.466737	0.533263
Mass density	[kg m^{-3}]		463.78	1054.95

We present a detailed example of the phase-equilibrium computation for a ternary system from Example 3 to demonstrate both the increase and decrease in the number of phases. It can be observed that passing through the three-phase region allows to escape from a local minimum in two-phase flash and eventually find another two-phase state with lower energy. In this example, we also provide information about the numbers of iterations.

In the previous work [9], the non-uniqueness in determining the equilibrium state using the *PT* variables has been observed only in pure components at saturation pressure in two phases. Extending the results to three phases for CO_2–H_2O system under geologic carbon storage conditions, the behaviour similar to that of pure components has been observed in [10]. In this work, we provide several examples of binary or multicomponent mixtures exhibiting the same behaviour in three- or even four-phase region showing non trivial mixtures for which volume is not a unique function of pressure, temperature, and moles, or is extremely sensitive to small pressure changes. We have indicated that this can cause numerical difficulties when the *PT*-flash is used as a part of a compositional simulator. In this situation, the *VT*-specification is a well conditioned formulation providing robustness of the computation.

Acknowledgements

The work was supported by the projects LH12064 Computational Methods in Thermodynamics of Hydrocarbon Mixtures of the Ministry of Education of the Czech Republic.

Appendix A. Equations of state

In this work we use in Examples 1–4 the Peng–Robinson equation of state [28] in the form

$$P(V,T,N_1,\ldots,N_n)=\frac{NRT}{V-\mathcal{B}}-\frac{\mathcal{A}}{V^2+2\mathcal{B}V-\mathcal{B}^2},$$

where R is the universal gas constant, $N=\sum_{i=1}^{n}N_i$ is the total mole number, and coefficients $\mathcal{A}$ and $\mathcal{B}$ are given by

$$\begin{aligned}
\mathcal{A} &= \sum_{i=1}^{n}\sum_{j=1}^{n}N_iN_ja_{ij}, \quad \mathcal{B}=\sum_{i=1}^{n}N_ib_i,\\
a_{ij} &= (1-\delta_{i-j})\sqrt{a_ia_j}, \quad b_i=0.0778\frac{RT_{i,crit}}{P_{i,crit}},\\
a_i &= 0.45724\frac{R^2T_{i,crit}^2}{P_{i,crit}}[1+m_i(1-\sqrt{T_{r,i}})]^2, \quad T_{r,i}=\frac{T}{T_{i,crit}},\\
m_i &= \begin{cases} 0.37464+1.54226\omega_i-0.26992\omega_i^2, & \text{for } \omega_i<0.5,\\ 0.3796+1.485\omega_i-0.1644\omega_i^2+0.01667\omega_i^3 & \text{for } \omega_i\geq 0.5.\end{cases}
\end{aligned}$$

In these equations δ_{i-j} denotes the binary interaction parameter between the components i and j, $T_{i,crit}$, $P_{i,crit}$, and ω_i are the critical temperature, critical pressure, and accentric factor of the i-th component, respectively.

In Examples 5 and 6 we use for the mixtures with water (H_2O) the Cubic-Plus-Association (CPA) equation of state [6,13]. This equation uses the Peng–Robinson equation of state for the physical interactions and the thermodynamic perturbation theory for the bonding of water molecules. Consider a mixture of n components containing water (H_2O) with mole number N_1 and nonwater species such as linear alkanes (methane, ethane, etc.), 1-alkenes (ethene, propene, etc.), aromatic hydrocarbons (containing benzene ring), H_2S, CO_2 or N_2 with moles $N_2,\ldots,N_n$. We assume that each water molecule has four association sites of two types (mark them α and β), so each type has two sites. We assume the same for each molecule of nonwater species (call them pseudo-associating components), whose association sites can be marked as α'_i and β'_i, where $i\in\{2,\ldots,n\}$. Let χ_α and χ_β be the mole fractions of water not bonded at site α and β, respectively, and let $\chi_{\alpha'_i}$ and $\chi_{\beta'_i}$ be the mole fractions of pseudo-associating component i not bonded at site α'_i and β'_i, respectively. Assuming neither cross association nor self association between any molecules of pseudo-associating components, i.e. the association strength $\Delta^{\alpha'_i\beta'_j}=0$ for $i,j=2,\ldots,n$, and symmetric cross association between the two sites of different type of water and pseudo-associating component i, i.e. $\Delta^{\alpha\beta'_i}=\Delta^{\alpha'_i\beta}$, we obtain the following simplified expressions for the symmetric four-site association model [13]

$$\begin{aligned}
\chi_\alpha=\chi_\beta=\chi_1 &= \frac{1}{1+2\frac{N_1}{V}\chi_1\Delta^{\alpha\beta}+\sum_{i=2}^{n}2\frac{N_i}{V}\chi_i\Delta^{\alpha\beta'_i}},\\
\chi_{a'_i}=\chi_{\beta'_i}=\chi_i &= \frac{1}{1+2\frac{N_1}{V}\chi_1\Delta^{\alpha\beta'_i}}, \qquad i=2,\ldots,n
\end{aligned}$$

In these equations, the association strength between molecules of water is given by

$$\Delta^{\alpha\beta}=g\kappa^{\alpha\beta}[\exp(\epsilon^{\alpha\beta}/k_BT-1)],$$

where k_B is the Boltzmann constant, $\kappa^{\alpha\beta}$ and $\epsilon^{\alpha\beta}$ are the bonding volume and energy parameters of water, respectively, and g is the contact value of the radial distribution function of hard-sphere mixture that can be approximated as $g=g(\eta)\approx\frac{1-0.5\eta}{(1-\eta)^3}$, where $\eta=\mathcal{B}/4V$. The association strength between water and pseudo-associating component i is related to the strength between water molecules as $\Delta^{\alpha\beta'_i}=s_i\Delta^{\alpha\beta}$ where s_i is the temperature-dependent cross association coefficient which can be determined together with the binary interaction coefficient δ_{i-j} by fitting the experimental data. If $s_i=0$ for some i, the cross association between water and i-th component is neglected. As a result, the CPA equation of state for mixtures of n components, i.e. water and nonwater pseudo-associating species, is given by

$$\begin{aligned}
P(V,T,N_1,N_2,\ldots,N_n) = &\frac{NRT}{V-\mathcal{B}}-\frac{\mathcal{A}}{V^2+2\mathcal{B}V-\mathcal{B}^2}\\
&+2RT\Big(\frac{\eta}{g}\frac{\partial g}{\partial\eta}+1\Big)\sum_{i=1}^{n_{cross}}\Big[\frac{N_i}{V}(\chi_i-1)\Big],
\end{aligned}$$

where R is the universal gas constant, $\mathcal{A}$ and $\mathcal{B}$ are the parameters from the Peng–Robinson equation of state, n_{cross} is the number of pseudo-associating components for which the cross association coefficient $s_i\neq 0$, $N=\sum_{i=1}^{n}N_i$ is the total mole number, and $\frac{\partial g}{\partial\eta}=\frac{2.5-\eta}{(1-\eta)^4}$. The coefficients a_i and b_i for water (marking water as the first component in the mixture) read as

$$\begin{aligned}
a_1 &= c_0\left[1.0+c_1\left(1-\sqrt{T_{r,1}}\right)+c_2\left(1-\sqrt{T_{r,1}}\right)^2+c_3\left(1-\sqrt{T_{r,1}}\right)^3\right]^2,\\
b_1 &= 1.45843\cdot 10^{-5},
\end{aligned}$$

where $T_{r,1}$ is the reduced temperature of water, which was defined above, and c_0, c_1, c_2, c_3 are the parameters of the equation of state given in Table 5.

Appendix B. Cholesky factorization

A symmetric positive definite matrix $\mathbb{A}\in\mathbf{R}^{n\times n}$ can be written as

$$\mathbb{A}=\mathbb{L}\mathbb{D}\mathbb{L}^T,$$

where $\mathbb{L}$ is a unit lower triangular matrix with all diagonal elements equal to one, and $\mathbb{D}$ is a diagonal matrix with strictly positive elements. This factorization is called the Cholesky factorization. Writing the above equation as

$$\begin{pmatrix} a_{11} & a_{12} & \dots & a_{1n} \\ a_{21} & a_{22} & \dots & a_{2n} \\ \vdots & \vdots & \ddots & \vdots \\ a_{n1} & a_{n2} & \dots & a_{nn} \end{pmatrix} = \begin{pmatrix} 1 & & & \\ l_{21} & 1 & & \\ \vdots & \vdots & \ddots & \\ l_{n1} & l_{n2} & \dots & 1 \end{pmatrix} \begin{pmatrix} d_{11} & & & \\ & d_{22} & & \\ & & \ddots & \\ & & & d_{nn} \end{pmatrix} \begin{pmatrix} 1 & l_{21} & \dots & l_{n1} \\ & 1 & \dots & l_{n2} \\ & & \ddots & \vdots \\ & & & 1 \end{pmatrix},$$

it can be seen that the j-th column of the matrices $\mathbb{D}$ and $\mathbb{L}$ can be computed directly from columns 1 to $j-1$ of the matrix $\mathbb{A}$ as

$$d_{jj} = a_{jj} - \sum_{k=1}^{j-1} d_{kk} l_{jk}^2,$$
$$l_{ij} = \frac{1}{d_{jj}} (a_{ij} - \sum_{k=1}^{j-1} d_{kk} l_{jk} l_{ik}).$$

If the matrix $\mathbb{A}$ is positive definite, then all its leading principal minors are positive, a unique Cholesky decomposition exists, and the decomposition is stable [7].

If the matrix $\mathbb{A}$ is not positive definite, then the Cholesky decomposition need not exist or may be unstable. The positive definiteness of $\mathbb{A}$ is not tested a priori. The usual Cholesky decomposition is attempted, and if a non-positive (or even a too small positive) element appears on the diagonal of $\mathbb{D}$ in the course of the Cholesky decomposition, then the corresponding diagonal element of $\mathbb{A}$ is modified to a sufficiently large positive value to ensure that all the diagonal elements of matrix $\mathbb{D}$ are positive. This way we obtain a Cholesky factorization of a matrix

$$\hat{\mathbb{A}} = \mathbb{A} + \mathbb{E} = \mathbb{L}\mathbb{D}\mathbb{L}^T,$$

that is symmetric and positive definite and differs from the original matrix $\mathbb{A}$ by matrix $\mathbb{E}$, which is non-negative and diagonal. The matrix $\hat{\mathbb{A}}$ can be used in the Newton method instead of $\mathbb{A}$. Having the Cholesky decomposition of $\hat{\mathbb{A}}$ available, the systems with matrix $\hat{\mathbb{A}}$ can be solved readily. The modification of the diagonal elements of $\mathbb{A}$ is performed so that all elements of $\mathbb{D}$ are strictly positive and the elements of $\mathbb{L}$ satisfy a uniform bound

$$d_{kk} > \delta \quad \text{and} \quad |l_{ik}\sqrt{d_{kk}}| \le \beta, \quad i > k,$$

where β is a positive value. Moreover, to reduce the norm of the modification, symmetric interchanges may be used; at the j-th step of the factorization the j-th row and column are chosen as those with the largest value of the diagonal element.

The essential steps of the modified Cholesky algorithm from [7] are described below.

B.1. Modified Cholesky factorization

Step 1 [Compute the bound on the elements of the matrices $\mathbb{L}$ and $\mathbb{D}$] Set $\beta^2 = \max\{\gamma, \xi/\nu, \epsilon_M\}$ where ϵ_M is the machine precision, γ and ξ are the maximum magnitudes of the diagonal and off-diagonal elements of the matrix $\mathbb{A}$, and $\nu = \max\{1, \sqrt{n^2-1}\}$.

Step 2 [Initialize] Set the column index $j = 1$. Define auxiliary quantities $c_{ii} = a_{ii}$, $i = 1, \dots, n$.

Step 3 [Find the maximum prospective diagonal and perform row and column interchanges] Find the smallest index q such that $|c_{qq}| = \max_{j \le i \le n} |c_{ii}|$. Interchange all information corresponding to rows and columns q and j of matrix $\mathbb{A}$.

Step 4 [Compute the j-th row of $\mathbb{L}$. Find the maximum modulus of $l_{ij}d_{jj}$] Set $l_{jk} = c_{jk}/d_{kk}$ for $k = 1, \dots, j-1$. Compute the quantities $c_{ij} = a_{ij} - \sum_{k=1}^{j-1} l_{jk}c_{ik}$ for $i = j+1, \dots, n$ and set $\theta_j = \max_{j+1 \le i \le n} |c_{ij}|$ (if $j = n$, define $\theta_j = 0$).

Step 5 [Compute the j-th diagonal element of $\mathbb{D}$] Define $d_{jj} = \max\{\delta, |c_{jj}|, \theta_j^2/\beta^2\}$, where δ is a small positive number (in this work, $\delta = 10^{-3}$), and the diagonal modification $e_{jj} = d_{jj} - c_{jj}$. If $j = n$, exit.

Step 6 [Update the prospective diagonal elements and the column index] Set $c_{ii} = c_{ii} - c_{ij}^2/d_{jj}$, for $i = j+1, \dots, n$. Set j to $j+1$ and go to Step 3.

List of notation.

Symbol	Meaning
A	Helmholtz energy
b_i	Covolume parameter of the Peng–Robinson EOS
c	Molar density
δ_{X-Y}	Binary interaction coefficient between components X and Y
i, j	Component indices
k	Iteration index
μ_i	Chemical potential of the i-th component
$M_{w,i}$	Molar weight of the i-th component
n	Number of components
N_i	Mole number of the i-th component
ω_i	Accentric factor of the i-th component
P	Pressure
$P_{i,crit}$	Critical pressure of the i-th component
Π	Number of phases
R	Universal gas constant
T	Absolute temperature
$T_{i,crit}$	Critical temperature of the i-th component
V	Total volume of the system
z_i	Overall molar fraction of the i-th component

References

[1] V. Alvarado, E. Manrique, Enhanced oil recovery: an update review, Energies 3 (2010) 1529–1575.
[2] V.F. Cabral, M. Castier, F.W. Tavares, Thermodynamic equilibrium in systems with multiple adsorbed and bulk phases, Chem. Eng. Sci. 60 (2005) 1773–1782.
[3] M. Castier, F.W. Tavares, Centrifugation equilibrium of natural gas, Chem. Eng. Sci. 60 (2005) 2927–2935.
[4] Z. Chen, G. Huan, Y. Ma, Computational Methods for Multiphase Flows in Porous Media, SIAM Philadelphia, 2006.
[5] R.O. Espósito, M. Castier, F.W. Tavares, Calculations of thermodynamic equilibrium in systems subject to gravitational fields, Chem. Eng. Sci. 55 (2000) 3495–3504.
[6] A. Firoozabadi, Thermodynamics of Hydrocarbon Reservoirs, McGrew-Hill, 1999.
[7] P.E. Gill, W. Murray, M.H. Wright, Practical Optimization, Academic Press, 1997.
[8] H. Hoteit, A. Firoozabadi, Compositional modeling by the combined discontinuous Galerkin and mixed methods, SPE J. (March) (2006) 19–34.
[9] T. Jindrová, J. Mikyška, Fast and robust algorithm for calculation of two-phase equilibria at given volume, temperature, and moles, Fluid Phase Equilib. 353 (2013) 101–114.
[10] T. Jindrová, J. Mikyška, Phase equilibria calculation of CO_2–H_2O system at given volume, temperature, and moles in CO_2 sequestration, IAENG J. Appl. Math. (2013) (in press).

[11] T. Jindrová, Computational Methods in Thermodynamics of Multicomponent Mixtures, Master degree thesis, Czech Technical University in Prague, 2013.
[12] A.M.M. Leal, M.J. Blunt, T.C. LaForce, A robust and efficient numerical method for multiphase equilibrium calculations: application to CO_2-brine-rock systems at high temperatures, pressures and salinities, Adv. Water Resour. 62 (2013) 409–430.
[13] Z. Li, A. Firoozabadi, Cubic-plus-association (CPA) equation of state for water-containing mixtures: Is 'cross association' necessary? AIChE J. 55 (7) (2009) 1803–1813.
[14] Z. Li, A. Firoozabadi, Modeling asphaltene precipitation by *n*-alkanes from heavy oils and bitumens using cubic-plus-association equation of state, Energy Fuels 24 (2010) 1106–1113.
[15] Z. Li, A. Firoozabadi, Cubic-plus-association equation of state for asphaltene precipitation in live oils, Energy Fuels 24 (2010) 2956–2963.
[16] Z. Li, A. Firoozabadi, General Strategy for Stability Testing and Phase-Split Calculation in Two and Three Phases, SPE Journal 17 (4) (2012) 1096–1107.
[17] M.L. Michelsen, The isothermal flash problem. 1. Stability, Fluid Phase Equilib. 9 (1982) 1–19.
[18] M.L. Michelsen, The isothermal flash problem. 2. Phase-split computation, Fluid Phase Equilib. 9 (1982) 21–40.
[19] M.L. Michelsen, J.M. Mollerup, Thermodynamic Models: Fundamentals and Computational Aspects, Tie-Line Publications, 2004.
[20] M.L. Michelsen, State function based flash specifications, Fluid Phase Equilib. 158 (1999) 617–626.
[21] J. Mikyška, A. Firoozabadi, Implementation of higher-order methods for robust and efficient compositional simulation, J. Computat. Phys. 229 (8) (2010) 2898–2913.
[22] J. Mikyška, A. Firoozabadi, A new thermodynamic function for phase-splitting at constant temperature moles and volume, AIChE J. 57 (7) (2011) 1897–1904.
[23] J. Mikyška, A. Firoozabadi, Investigation of mixture stability at given volume, temperature, and number of moles, Fluid Phase Equilib. 321 (2012) 1–9.
[24] J. Moortgat, Z. Li, A. Firoozabadi, Three-phase compositional modeling of CO_2 injection by higher-order finite element methods with CPA equation of state for aqueous phase, Water Resour. Res. 48 (12) (2012) W12511, http://dx.doi.org/10.1029/2011WR011736/.
[25] J. Moortgat, S. Sun, A. Firoozabadi, Compositional modeling of three-phase flow with gravity using higher-order finite element methods, Water Resour. Res. 47 (2011) W05511, http://dx.doi.org/10.1029/2010WR009801.
[26] N.R. Nagarajan, A.S. Cullick, New strategy for phase equilibrium and critical point calculations by thermodynamic energy analysis. Part I. Stability analysis and flash, Fluid Phase Equilibria 62 (3) (1991) 191–210.
[27] N.R. Nagarajan, A.S. Cullick, New strategy for phase equilibrium and critical point calculations by thermodynamic energy analysis. Part II. Critical point calculations, Fluid Phase Equilibria 62 (3) (1991) 211–223.
[28] D.Y. Peng, D.B. Robinson, A New Two-Constant Equation of State, Ind. Eng. Chem.: Fundam. 15 (1976) 59–64.
[29] F.E. Pereira, A. Galindo, G. Jackson, C.S. Adjiman, On the impact of using volume as an independent variable for the solution of P-T fluid phase equilibrium with equations of state, Comp. Chem. Eng. 71 (2014) 67–76.
[30] O. Polívka, J. Mikyška, Compositional modeling in porous media using constant volume flash and flux computation without the need for phase identification, J. Computat. Phys. 272 (2014) 149–179.
[31] A. Quaternioni, R. Sacco, F. Saleri, Numerical Mathematics, Springer, 2000.
[32] H. Zhang, A. Bonilla-Petricionet, G.P. Rangaiah, A review on global optimization methods for phase equilibrium modeling and calculations, Open Thermodyn. J. 5 (S1) (2011) 71–92.